The Cryosphere Discuss., 7, 2191–2245, 2013
www.the-cryosphere-discuss.net/7/2191/2013/
doi:10.5194/tcd-7-2191-2013

The Cryosphere Discussions
Open Access

Simulation of wind-induced snow transport in alpine terrain using a fully coupled snowpack/atmosphere model

V. Vionnet[1], E. Martin[1], V. Masson[1], G. Guyomarc'h[2], F. Naaim-Bouvet[3], A. Prokop[4], Y. Durand[2], and C. Lac[1]

[1]Météo-France/CNRS, CNRM – GAME UMR3589, Toulouse, France
[2]Météo-France/CNRS, CNRM – GAME UMR3589, CEN, St. Martin d'Hères, France
[3]IRSTEA, UR ETNA, St. Martin d'Hères, France
[4]Institue of Mountain Risk Engineering, University of Natural Resources and Applied Life Sciences, Wien, Austria

Received: 6 May 2013 – Accepted: 20 May 2013 – Published: 3 June 2013

Correspondence to: V. Vionnet (vincent.vionnet@meteo.fr)

Published by Copernicus Publications on behalf of the European Geosciences Union.

Abstract

In alpine regions, wind-induced snow transport strongly influences the spatio-temporal evolution of the snow cover throughout the winter season. To gain understanding on the complex processes that drive the redistribution of snow, a new numerical model is developed. It couples directly the detailed snowpack model Crocus with the atmospheric model Meso-NH. Meso-NH/Crocus simulates snow transport in saltation and in turbulent suspension and includes the sublimation of suspended snow particles. A detailed representation of the first meters of the atmosphere allows a fine reproduction of the erosion and deposition process. The coupled model is evaluated against data collected around the experimental site of Col du Lac Blanc (2720 m a.s.l., French Alps). For this purpose, a blowing snow event without concurrent snowfall has been selected and simulated. Results show that the model captures the main structures of atmospheric flow in alpine terrain, the vertical profile of wind speed and the snow particles fluxes near the surface. However, the horizontal resolution of 50 m is found to be insufficient to simulate the location of areas of snow erosion and deposition observed by terrestrial laser scanning. When activated, the sublimation of suspended snow particles causes a reduction in deposition of 5.3 %. Total sublimation (surface + blowing snow) is three times higher than surface sublimation in a simulation neglecting blowing snow sublimation.

1 Introduction

Wind-induced snow transport is an important component of the interaction between the cryosphere and the atmosphere. It occurs in regions seasonally or permanently covered by snow. In alpine terrain, snow transport creates inhomogeneous snow depth distribution, strongly influenced by the local topography (e.g. Föhn, 1980; Durand et al., 2005; Mott et al., 2010). Snow is eroded in area exposed to strong wind (crest for example) and is deposited in area sheltered from the wind. This has a major influence on the evolution of the avalanche danger (Schweizer et al., 2003; Guyomarc'h et al., 2008).

TCD
7, 2191–2245, 2013

Cornices and wind slabs result indeed from the deposition of small rounded grains during blowing snow events and their formation affect the snowpack stability (Meister, 1989). Wind-induced snow transport has also hydrological consequences since part of the transported snow mass is lost by sublimation (e.g. Strasser et al., 2008; MacDonald et al., 2010; Groot Zwaaftink et al., 2011).

Wind-induced snow transport occurs when the wind speed exceeds a threshold value that depends on the snow type at the surface (Schmidt, 1980; Guyomarc'h and Mérindol, 1998; Lehning et al., 2000). Three modes of snow transport are generally identified: reptation, saltation and turbulent suspension. Reptation corresponds to the rolling of particles over the surface of the snowpack and its contribution is negligible compared to the other processes (Kosugi et al., 1992). It is commonly neglected in blowing snow models. In saltation, particles follow ballistic trajectories in a shallow layer close to the ground. When returning to the surface, they may rebound and/or eject new grains. Turbulent suspension occurs in the atmosphere above the saltation layer where snow grains are transported by turbulent eddies without contact with the surface. Distances of transport are limited by the sedimentation and sublimation of snow grains. The later process modifies the vertical profiles of temperature and humidity in the surface boundary layer (Schmidt, 1982; Déry et al., 1998).

Several models have been developed to simulate wind-induced snow redistribution in alpine terrain and resulting snow-depth pattern (e.g. Naaim et al., 1998; Gauer, 1999; Durand et al., 2005; Liston et al., 2007; Lehning et al., 2008; Schneiderbauer and Prokop, 2011). These models are generally made of two components: (i) a snowpack component to estimate the threshold wind speed for snow transport and the erodible snow mass and (ii) an atmospheric component to simulate at high resolution the spatial and temporal evolution of the wind field and the resulting snow transport. They cover a wide range of complexity depending if they are dedicated to simulate single blowing snow event or the entire snow season (Liston et al., 2007).

Simulating wind-induced snow transport in alpine terrain requires primarily a good knowledge of the high-resolution wind field over complex topography. Crest speed-up,

TCD
7, 2191–2245, 2013

flow channeling or the formation of recirculation zone are indeed the driving mechanisms behind the inhomogeneous snow distribution resulting from blowing snow events (e.g. Lehning et al., 2008; Mott and Lehning, 2010; Schneiderbauer and Prokop, 2011). To reproduce such features, the more advanced snow transport models use three-dimensional wind fields. They are computed by models of computational fluid dynamics (Gauer, 1999; Schneiderbauer and Prokop, 2011) or atmospheric models run in the Large Eddy Simulation (LES) mode. Bernhardt et al. (2009) combined for example wind fields from the MM5 atmospheric model (Grell et al., 1995) at an horizontal resolution of 200 m with the snow-transport model of Liston et al. (2007). In a further study, Bernhardt et al. (2010) used kinematic downscaling to refine MM5 wind fields from 200 to 30 m. The atmospheric model ARPS (Xue et al., 2000) provided wind fields at an horizontal grid spacing down to 5 m (Mott and Lehning, 2010; Mott et al., 2010) to drive the snow transport module of Alpine3D (Lehning et al., 2008).

In alpine terrain, the atmospheric models previously mentioned are used to drive snow transport models and do not simulate interactively drifting and blowing snow. The driving wind fields are extracted from wind field libraries and kept constant for a given time step (1 h for example in the model of Lehning et al., 2008). Until now, the interactive simulation of snow transport has been only implemented in regional climate models applied over large areas at horizontal resolution higher than 5 km (Gallée et al., 2001; Déry and Yau, 2001b; Lenaerts et al., 2012). However, previous works have shown that atmospheric models can be run at high resolution in complex terrain to simulate interactively meteorological situations such as flow in a steep valley (Weigel et al., 2006, resolution of 150 m) or scalar dispersion (Michioka and Chow, 2008, resolution of 25 m). These studies were successful at capturing the flow structures in complex terrain and brought understanding of the atmospheric processes at stake in this environment. As a consequence, such configurations can be applied to the interactive simulation of blowing snow events in alpine terrain.

In this study, we introduce a new coupled model to simulate blowing snow events in alpine terrain and resulting snow redistribution. The atmospheric component is made

TCD
7, 2191–2245, 2013

of the atmospheric model Meso-NH (Lafore et al., 1998) to simulate interactively the evolution of meteorological conditions and resulting snow transport. At the bottom of the atmosphere, the latest version of the detailed snowpack model Crocus (Brun et al., 1989, 1992; Vionnet et al., 2012a) describes snowpack properties. Examples of problems that can be better investigate with fully coupled snowpack/atmosphere simulations of blowing snow events in alpine terrain include (1) the importance of blowing snow sublimation and its feedback on the atmospheric boundary layer (Strasser et al., 2008; MacDonald et al., 2010; Groot Zwaaftink et al., 2011), (2) the use of grid nesting techniques to provide realistic boundary conditions to local atmospheric simulation (resolution ≈ 50 m) (e.g. Liu et al., 2011; Talbot et al., 2012) and (3) the relative contribution of preferential deposition of snowfall and wind-induced snow transport to the spatial variability of the mountainous snowcover (Lehning et al., 2008; Dadic et al., 2010; Mott et al., 2010).

Our paper describes the new snow transport model Meso-NH/Crocus. It is evaluated against a full set of observations collected during a blowing snow event at the experimental site of Col du Lac Blanc (French Alps). Our paper is organized as follows. Section 2 describes the two components of the coupled snowpack/atmosphere model. Then, Sect. 3 presents the new drifting and blowing snow scheme included in the coupled model. Section 4 gives additional information regarding Col du Lac Blanc and the model configuration used to simulated the selected blowing snow event. Finally, Sect. 5 provides a large evaluation of Meso-NH/Crocus in terms of simulation of atmospheric flow in complex terrain, blowing snow fluxes and reproduction of patterns of snow erosion and deposition. The influence of blowing snow sublimation is also discussed in Sect. 5.

TCD
7, 2191–2245, 2013

2 Model descriptions

2.1 Atmospheric model

We use the meso-scale, nonhydrostatic atmospheric model Meso-NH. This model has been jointly developed by CNRM (Météo-France) and Laboratoire d'Aérologie (CNRS) (Lafore et al., 1998). Meso-NH can simulate fine scale (LES type) to synoptic scale (horizontal resolution ranging from a few meters to several tens of kilometers) and can run in two-way nested mode. For high-resolution simulations, the scheme of Cuxart et al. (2000) allows the computation of 3-D turbulence. Cloud developments and resulting precipitation (rainfall and snowfall) are simulated by the bulk microphysical scheme of Pinty and Jabouille (1998).

Meso-NH has been previously applied in alpine terrain during the Mesoscale Alpine Program (e.g. Bougeault et al., 2001; Stein, 2004). Studies were carried out at sub-kilometic resolution (0.3–1 km) and focused on Foehn flow (Beffrey et al., 2004) or orographic precipitations (Lascaux et al., 2006). More recently, Brun and Chollet (2010) showed that Meso-NH is suitable to simulate wind field evolution over complex terrain at high resolution (down to 10 m).

2.2 Snow model

Meso-NH is coupled to the externalized surface module SURFEX which handles energy and mass fluxes between the atmosphere and the surface (Masson et al., 2012). SURFEX includes in particular the land surface scheme ISBA (Interactions between Soil, Biosphere, and Atmosphere, Noilhan and Planton, 1989) which represents the snowpack through several schemes of increasing complexity. In this study, we use SURFEX/ISBA-Crocus (referred later as Crocus), the latest version of the snowpack scheme Crocus (Brun et al., 1989, 1992) which has been recently implemented in SURFEX (Vionnet et al., 2012a). Crocus has been run operationnaly for avalanche

TCD
7, 2191–2245, 2013

forecasting over the French mountains for 20 yr (Durand et al., 1999). Previous versions of Crocus has also been used in snow transport models (Durand et al., 2001, 2005).

Crocus is a one-dimensional multi-layer snow scheme. It simulates the evolution of the snowpack as a function of energy and mass-transfer between the snowpack and the atmosphere (radiative balance, turbulent heat and moisture transfer, precipitation) and the snowpack and the ground below (ground heat flux). One important feature of the model is its ability to simulate snow metamorphism through a comprehensive set of semi-empirical laws. The type and size of the crystals of each layer of the snowpack are prognostic variables, which control the surface albedo and the compaction rate of the different layers. A complete description of the model can be found in Vionnet et al. (2012a).

3 Treatment of drifting and blowing snow

We have implemented new specific routines within the coupled system Meso-NH/Crocus to handle wind-induced snow transport. As in earlier-developed models (e.g. Gauer, 1999; Durand et al., 2005; Liston et al., 2007; Lehning et al., 2008), snow transport is divided into turbulent suspension and saltation. Figure 1 shows an overview of the new blowing snow scheme which is made of three main components: (i) a specific scheme implemented in Meso-NH simulates snow transport in turbulent suspension, (ii) dedicated routines in SURFEX determine blowing snow occurrence and simulate snow transport in saltation and (iii) mass exchanges between the snowpack and the atmosphere are computed through an adapted version of the surface boundary layer (SBL) scheme Canopy (Masson and Seity, 2009). Details concerning each component are given in the following subsections while Appendix A contains a summary of the variables and units used by the model.

TCD
7, 2191–2245, 2013

3.1 Suspension layer

3.1.1 Particle size distribution (PSD)

Several field experiments have shown that the size distribution of blown snow particles in the atmosphere is satisfyingly represented by a two-parameter gamma distribution (Budd, 1966; Dover, 1993; Nishimura and Nemoto, 2005; Gordon and Taylor, 2009; Naaim-Bouvet et al., 2011). The snow particle size distribution (PSD) follows:

$$n(r) = \frac{N_s \rho_{\text{air}} r^{\alpha-1} \exp(-r/\beta)}{\beta^{\alpha} \Gamma(\alpha)} \quad (1)$$

where N_s is the number of particles per unit of mass (kg^{-1}), ρ_{air} the air density (kg m^{-3}), r is the particle radius (m) and Γ the Gamma function. α (–) and β (m) denote the shape and scale parameters of the distribution. The average radius, r_{m}, is given by $r_{\text{m}} = \alpha\beta$.

In our model, we consider blown snow particles as spherical. Such assumption is used by many blowing snow models that include a PSD (Mann, 1998; Bintanja, 2000; Déry and Yau, 2001a; Yang and Yau, 2008). Under the spherical assumption, the mixing ratio of blowing snow q_{s} (kg kg^{-1}) can be expressed as:

$$q_{\text{s}} = \frac{4\pi\rho_{\text{ice}}}{3\rho_{\text{air}}} \int_0^{\infty} r^3 n(r) \text{d}r \quad (2)$$

where ρ_{ice} is the ice density (kg m^{-3}). Integrating Eq. (2) using the expression given in Eq. (1) for $n(r)$, we get:

$$\beta = \left[\frac{3 q_{\text{s}} \Gamma(\alpha)}{4\pi\rho_{\text{ice}} \Gamma(\alpha+3) N_s} \right]^{1/3} \quad (3)$$

We follow the work of Déry and Yau (2001a) and use a double-moment scheme to represent the temporal and spatial evolution of the two-parameter gamma distribution

TCD
7, 2191–2245, 2013

of snow in suspension. Such approach predicts the evolution of the number concentration per unit of mass, N_s, and mixing ratio, q_s, of blown snow particles and requires a specified value of α. β is then solved using Eq. (3). This approach allows the model to account for spatio-temporal variations of r_m and its effects on the sedimentation and sublimation terms. Note that our double-moment scheme differs from the microphysical scheme of Meso-NH (Pinty and Jabouille, 1998) contrary to the approach of Gallée et al. (2001) who make no distinction between blown snow particles and snowflakes despite differences of shape and size (Nishimura and Nemoto, 2005).

3.1.2 Prognostic equations

The equation for N_s and q_s depends on space variables x_i and time t following:

$$\underbrace{\frac{\partial N_s}{\partial t} + u_j \frac{\partial N_s}{\partial x_j}}_{\text{Adv}} = \underbrace{-\frac{\partial}{\partial x_j}\left(\overline{N_s' u_j'}\right)}_{\text{Turb}} + \underbrace{\frac{\partial}{\partial x_j}\left(N_s V_N \delta_{j3}\right)}_{\text{Sedim}} + \underbrace{S_N}_{\text{Subl}} \tag{4}$$

$$\underbrace{\frac{\partial q_s}{\partial t} + u_j \frac{\partial q_s}{\partial x_j}}_{\text{Adv}} = \underbrace{-\frac{\partial}{\partial x_j}\left(\overline{q_s' u_j'}\right)}_{\text{Turb}} + \underbrace{\frac{\partial}{\partial x_j}\left(q_s V_q \delta_{j3}\right)}_{\text{Sedim}} + \underbrace{S_q}_{\text{Subl}} \tag{5}$$

where Adv denotes the advection term and Turb the turbulence term. Sedim indicates the sedimentation term and Subl represents the sink term associated to sublimation for N_s and q_s. **u** is the 3-D wind vector, V_N and V_q are the number- and mass-weighted mean particle fall speeds.

The advection of N_s and q_s is handled by specific routines of Meso-NH dedicated to the advection of meteorological variables. It relies on the Piecewise Parabolic Method (Colella and Woodward, 1984; Carpenter et al., 1990). The flux limiter of Skamarock (2006) ensures monotonicity preservation.

The 3-D turbulent scheme of Meso-NH (Cuxart et al., 2000) computes the turbulent diffusion of N_s and q_s. This scheme solves a prognostic equation for the turbulent

TCD
7, 2191–2245, 2013

kinetic energy, e_{TKE}. Turbulent fluxes are then computed following a 1.5 closure. In our model, turbulent fluxes of blowing snow variables are proportional to the turbulent fluxes of scalar variables. We define ζ as the ratio between the diffusion coefficient of scalar variables, K_{Sca}, and blowing snow variables, K_{Snw}. Thus, the turbulent flux $\overline{q'_s u'_j}$ is written:

$$\overline{q'_s u'_j} = -K_{\mathrm{Snw}} \frac{\partial q_s}{\partial x_j} = -\frac{K_{\mathrm{Sca}}}{\zeta} \frac{\partial q_s}{\partial x_j} \text{ with } K_{\mathrm{Sca}} = \frac{2}{3} \frac{L_m}{C_S} e_{\mathrm{TKE}}^{1/2} \Psi_j \tag{6}$$

where C_S and the stability function Ψ_j are taken from Redelsperger and Sommeria (1981). L_m denotes the mixing length. For 3-D simulations at high horizontal resolution (≤ 200 m), it depends on the mesh size and is limited by the mixing length of Deardorff (1972) in stable cases. Close to the surface, L_m follows the formulation of Redelsperger et al. (2001). A sensitivity study showed that the value $\zeta = 0.25$ allows to reproduce vertical profiles of blowing snow fluxes measured at Col du Lac Blanc over a large range of wind speed as discussed in Vionnet (2012).

The sedimentation terms in Eqs. (4) and (5) require the computation of the number-weighted and mass-weighted mean particle fall speed. These velocities depend on the PSD following:

$$V_N = \frac{\int_0^\infty v(r) n(r) \mathrm{d}r}{\int_0^\infty n(r) \mathrm{d}r} \tag{7}$$

$$V_q = \frac{\int_0^\infty v(r) r^3 n(r) \mathrm{d}r}{\int_0^\infty r^3 n(r) \mathrm{d}r} \tag{8}$$

where $v(r)$ denotes the fall speed for a particle of radius r and $n(r)$ the particle size distribution. $v(r)$ follows a quadratic equation derived by Dover (1993) based on a balance between the gravitational force acting on a spherical particle and the drag force

TCD
7, 2191–2245, 2013

using the drag coefficient proposed by Carrier (1953):

$$v(r) = -\frac{A}{r} + \sqrt{\left(\frac{A}{r}\right)^2 + Br} \text{ with } A = \frac{6.203\nu_{\text{air}}}{2} \text{ and } B = \frac{5.516\rho_{\text{ice}}}{4\rho_{\text{air}}}g \tag{9}$$

where ν_{air} ($\text{m}^2\,\text{s}^{-1}$) is the air viscosity and g ($\text{m}\,\text{s}^{-2}$) the acceleration due to gravity. Using this expression for $v(r)$, no analytical solution can be found for V_N and V_q so that the integrals in Eqs. (7) and (8) are solved numerically. To save computational time when 3-D simulations are performed, a model option allows the user to use pre-computed look-up tables of V_N and V_q function of the average radius r_{m} and the air pressure P_{air}.

3.1.3 Blowing snow sublimation

Sublimation terms appear in Eqs. (4) and (5). Indeed, when transported, suspended snow particles undergo sublimation if the ambient air is unsaturated with respect to ice. The sublimation of blowing snow acts as a sink of snow mass, a source of water vapor and a sink of sensible heat in the atmosphere. Several blowing snow models calculate sublimation rates of blown snow particles and account for the loss of mass due to sublimation (e.g. Déry et al., 1998; Bintanja, 2000; Liston and Sturm, 1998; Groot Zwaaftink et al., 2011). They all rely on the formulation of Thorpe and Mason (1966) that gives the mass change rate for a single ice sphere. Wever et al. (2009) showed that this formulation can be transferred to an ensemble of snow particles. Our model follows the same formulation.

Ignoring the influence of solar radiation, the sublimation rate of an ice sphere of radius r is:

$$\frac{\text{d}m}{\text{d}t} = \frac{2\pi r\sigma}{\frac{L_{\text{s}}}{K_{\text{air}}T_{\text{air}}\text{Nu}}\left(\frac{L_{\text{s}}}{R_{\text{v}}T_{\text{air}}} - 1\right) + \frac{R_{\text{v}}T_{\text{air}}}{D_{\text{v}}e_{\text{si}}\text{Sh}}} \tag{10}$$

TCD
7, 2191–2245, 2013

where $\sigma = (e - e_{si})/e_{si}$ is the water vapor deficit with respect to ice, with e and e_{si} the vapor pressure and its value at saturation over ice (Pa) at air temperature T_{air} (K). R_v denotes the gas constant for water vapor ($J\,kg^{-1}\,K^{-1}$), D_v is the molecular diffusivity of water vapor in air ($m^2\,s^{-1}$), K_{air} is the molecular thermal conductivity of the air ($J\,m^{-1}\,s^{-1}\,K^{-1}$), L_s is the latent heat of sublimation (J kg^{-1}). Nu and Sh are, respectively, the Nusselt and Sherwood numbers. Expressions for D and K are taken from Pruppacher et al. (1998).

The Nusselt and Sherwood numbers represent the heat and mass transfer between the ice particle and the atmosphere. They are related to the particle Reynolds number Re (Lee, 1975):

$$\mathrm{Nu} = \mathrm{Sh} = \begin{cases} 1.79 + 0.606\sqrt{Re} & \text{for } 0.7 < Re \leq 10 \\ 1.88 + 0.580\sqrt{Re} & \text{for } 10 < Re < 200 \end{cases} \quad \text{with } Re = \frac{2rV_v}{\nu_{air}} \tag{11}$$

where V_v is the ventilation speed defined as the relative speed between the snow particle and the air. It is taken equal to the settling velocity of the particle given by Eq. (9) (Schmidt, 1982; Déry et al., 1998). This approach neglects ventilation effects associated with turbulence (Dover, 1993; Bintanja, 2000).

The total mass sublimation rate, S_q ($kg\,kg^{-1}\,s^{-1}$), in Eq. (5), is then obtained through integration over the particle size spectrum (Déry and Yau, 1999):

$$S_q = \frac{q_s \mathrm{Nu}(r_m)\sigma}{2\rho_{ice} r_m^2 A(T_{air}, P_{air})} \tag{12}$$

where $\mathrm{Nu}(r_m)$ is computed as in Eq. (11) with r_m for the radius and V_q for the settling velocity. The total number sublimation rate, S_N ($kg^{-1}\,s^{-1}$), is given by: $S_N = S_q N_s / q_s$ (Déry and Yau, 2001a). Sublimation feedbacks on the air are represented through additional terms proportional to S_b in the prognostic equations for vapor mixing ratio and potential temperature (Déry and Yau, 2001a; Groot Zwaaftink et al., 2011).

TCD
7, 2191–2245, 2013

3.2 Lower boundary condition and snowpack evolution

3.2.1 Occurrence of snow transport

The occurrence of snow transport is determined by the formulation of Guyomarc'h and Mérindol (1998) which gives the 5 m threshold wind speed, U_{5t}, as a function of snow grain type at the surface. The presence of a wet layer or a crust layer at the top of the snowpack prevents snow drifting. Vionnet et al. (2012b) found that this formulation predicts satisfactorily the occurrence of blowing snow events at an alpine site over a 10 yr period provided the mechanical fragmentation of snow grains during blowing snow events is taken into account. U_{5t} is then converted into a threshold friction velocity $u_{*\mathrm{th}}$ using the same method as Durand et al. (2005). Blowing snow occurs at grid points where the friction velocity u_* is higher than $u_{*\mathrm{th}}$. u_* is computed in SURFEX as a function wind speed at level of atmospheric forcing and transfer coefficient for momentum, $C_D : u_* = \sqrt{C_D} U_{\mathrm{Surf}}$. The expression of C_D accounts for thermal buoyancy effects (Louis, 1979) and does not include particle buoyancy effects (Bintanja, 2000; Gallée et al., 2001).

3.2.2 Saltation layer

The saltation layer develops where snow transport occurs. In our model, the saltation layer contributes to the total snow transport and acts as a lower boundary condition for the suspension layer.

Sørensen (2004) proposed a physically-based formulation for the horizontal transport rate, Q_{Salt} ($\mathrm{kg\,m^{-1}\,s^{-1}}$), of any particle in saltation:

$$Q_{\mathrm{Salt}} = \frac{\rho_{\mathrm{air}} u_*^3}{g}(1 - V^{-2})[a + bV^{-2} + cV^{-1}] \quad (13)$$

where $V = u_*/u_{*t}$. Constants a, b and c must be determined from observations (Sørensen, personal communication, 2012). For snow particles, we used the

TCD
7, 2191–2245, 2013

measurements of Nishimura and Hunt (2000) and found that $a = 2.6$, $b = 2.5$ and $c = 2$ allow to reproduce their observations. Doorschot and Lehning (2002) have similarly found a good agreement between mass fluxes simulated by their saltation model, derived from an earlier version of Eq. (13) (Sørensen, 1991) and observed by Nishimura and Hunt (2000).

Q_{Salt} is a stationary transport rate. Nemoto and Nishimura (2004) suggested that a time of 1–2 s is necessary to reach a steady state in the saltation layer. This corresponds to typical lengths of 1–20 m for wind speed close to the surface ranging from 1 to 10 $\mathrm{m\,s^{-1}}$. These lengths are lower than the targeted horizontal resolution of Meso-NH/Crocus (50 m in this study, see Sect. 4.2) so that we can use a stationary mass flux. The model of Lehning et al. (2008) use a similar assumption and manages to reproduce snow distribution down to an horizontal resolution of 5 m (Mott et al., 2010).

Mass exchanges between the saltation layer and the suspension layer requires the computation of a reference concentration, c_{Salt} ($\mathrm{kg\,m^{-3}}$), at the top of the saltation layer. The thickness of this layer is given by: $h_{\mathrm{Salt}} = 0.08436 u_*^{1.27}$ (Pomeroy and Male, 1992). c_{Salt} is then computed assuming an exponential decay of the mass flux in the saltation layer (Nishimura and Hunt, 2000):

$$c_{\mathrm{Salt}} = \frac{Q_{\mathrm{Salt}}}{u_{\mathrm{part}}} \frac{\lambda g}{u_*^2} \exp\left(-\frac{\lambda h_{\mathrm{Salt}} g}{u_*^2}\right) \tag{14}$$

where λ is a dimensionless parameter (0.45 for snow, Nishimura and Hunt, 2000). u_{part} denotes the horizontal particle velocity within the saltation layer which only depends on state of surface snow: $u_{\mathrm{part}} = 2.8 u_{*t}$ (Pomeroy and Gray, 1990). The corresponding number concentration, $\widetilde{N}_{\mathrm{salt}}$ ($\mathrm{m^{-3}}$), is then computed from c_{salt} assuming a two-parameter gamma distribution in the saltation layer and a fixed value for the average radius of particles in saltation, $r_{m\mathrm{Salt}}$.

TCD
7, 2191–2245, 2013

3.2.3 Snow erosion and accumulation

At each grid point, Meso-NH/Crocus computes a net mass flux, F_{Net} ($\mathrm{kg\,m^{-2}\,s^{-1}}$), between the snowpack and the atmosphere:

$$F_{\mathrm{Net}} = F_{\mathrm{Salt}} + F_{\mathrm{Susp}} + F_{\mathrm{Precip}} \tag{15}$$

where F_{Salt} and F_{Susp} denote the contribution of the transport in saltation and in turbulent suspension, respectively. F_{Precip} represents snowfall simulated by the microphysical scheme of Meso-NH (Pinty and Jabouille, 1998). Figure 2 summarized the mass exchanges between the snowpack and the atmosphere. Lehning et al. (2008) simulates snow erosion and deposition in a similar way. This method lacks the feedback of the suspension on the saltation concentration. A prognostic equation for snow concentration in saltation would be required to overcome this limitation as in Gauer (1999). The current version of the model uses the stationary assumption for the saltation layer.

The contribution from saltation corresponds to the divergence of the vector transport in saltation $\mathbf{Q}$:

$$F_{\mathrm{Salt}} = \nabla.\mathbf{Q} \text{ avec } \mathbf{Q} = Q_{\mathrm{Salt}} \frac{\boldsymbol{u}_{\mathbf{MNH}}}{\|\boldsymbol{u}_{\mathbf{MNH}}\|} \tag{16}$$

where $\boldsymbol{u}_{\mathbf{MNH}}$ is the wind vector at the first level of Meso-NH.

F_{Susp} is a net mass flux between the saltation layer and the lowest level of the atmosphere. It follows:

$$F_{\mathrm{Susp}} = F_{\mathrm{Sed}} - F_{\mathrm{Turb}} \tag{17}$$

where F_{Sed} is the sedimentation flux from the atmosphere and F_{Turb} the turbulent flux of blown snow particles towards the atmosphere. F_{Sed} corresponds to a loss of mass for the atmosphere:

$$F_{\mathrm{Sed}} = c_{\mathrm{Surf}} V_q \tag{18}$$

TCD
7, 2191–2245, 2013

where c_{Surf} denotes the near-surface concentration of blown snow particles (see Sect. 3.3) and V_q the mass-weighted mean fall speed at this level. The second term of Eq. (17) F_{Turb} follows the expression of Gallée et al. (2001):

$$F_{Turb} = U_{Surf} C_D (c_{Salt} - c_{Surf}) \quad (19)$$

where U_{Surf} denotes the near-surface wind speed (see Sect. 3.3). The computation of near-surface variables is detailed in the next section. Similar fluxes are computed for the number concentration using $\tilde{N}_{salt}$ and the near-surface number concentration $\tilde{N}_{surf}$.

Erosion occurs where $F_{Net} < 0$ and snow layers are removed from the snowpack profile simulated by Crocus. Therefore, snow layers with different characteristics may be exposed successively at the top of the snowpack during a blowing snow event. Snow accumulation is simulated where $F_{Net} > 0$. Deposited snow is added to the existing snowpack using the routines of Crocus handling the layering of the snowpack. The current version of the model use fixed values for the characteristics of deposited snow (Table 1). A future version of the model will account for the evolution of snow grain characteristics under snow transport.

3.3 Surface/atmosphere coupling

Mass fluxes between the snowpack and the atmosphere (Eqs. 18 and 19) require the estimation of near-surface variables (wind speed, U_{Surf}, and mass concentration, c_{Surf}). However, the vertical profile of blowing snow concentration exhibits strong gradient close to the surface (e. g. Budd, 1966; Mann, 1998; Gordon and Taylor, 2009). Therefore, an accurate estimation of mass fluxes requires a good reproduction of the vertical profile of blowing snow concentration close to the ground. For example, the 1-D blowing snow model of Mann (1998) uses a stretched grid with a first level at 10 cm above the surface and 70 levels in the lowest 100 m of the atmosphere. A similar configuration can be achieved with Meso-NH (even for 3-D configuration). Aumond et al. (2012) used for example 50 levels in the lowest 100 m of the atmosphere (lowest level at 50 cm) to simulate the drag effects of canopies. However, such configuration is not suitable to simulate

TCD
7, 2191–2245, 2013

atmospheric flow in alpine terrain where the presence of large slopes generates large vertical velocities and requires small time steps to avoid numerical instabilities.

An alternative solution is offered by the one-dimensional surface boundary layer (SBL) scheme Canopy (Masson and Seity, 2009). Canopy is implemented in SURFEX and includes prognostic atmospheric layers between the surface and the first level of Meso-NH. The evolution of SBL variables (wind, temperature, specific humidity and TKE) is resolved prognostically, taking into account large-scale forcing, turbulence, and, if any, drag and canopy forces and surface fluxes. These fluxes are computed between the surface and the lowest level of Canopy and sent back to the atmosphere. Therefore, Canopy allows to increase the vertical resolution near the ground in the surface scheme without the drawback of smaller time step. A complete description of Canopy is given in Masson and Seity (2009).

The prognostic variables N_s and q_s have been implemented in Canopy to reproduce the strong gradient of blowing snow concentration close to the ground. Their evolution are governed by the following one-dimensional equations:

$$\frac{\partial N_s}{\partial t} = \left(\frac{\partial N_s}{\partial t}\right)_{\text{Adv}} + \frac{\partial}{\partial z}\left(-\overline{N_s' w'} + V_N N_s\right) + S_N \tag{20}$$

$$\frac{\partial q_s}{\partial t} = \left(\frac{\partial q_s}{\partial t}\right)_{\text{Adv}} + \frac{\partial}{\partial z}\left(-\overline{q_s' w'} + V_q q_s\right) + S_q \tag{21}$$

The terms in these equations are similar to the terms appearing in Eqs. (4) and (5). The contribution of advection at each Canopy level is computed through the advection in Meso-NH of the total mass and total number of blown snow particles in Canopy. This procedure is detailed in Appendix B. The sublimation terms S_N and S_q are computed as a function of temperature and specific humidity at each Canopy levels. Feedbacks on the SBL are included by adding the contribution of blowing snow sublimation in Canopy to the sensible and latent heat fluxes emitted towards the atmosphere. This modifies in return the temperature and humidity at the lowest levels of Meso-NH and, therefore, at Canopy levels.

TCD
7, 2191–2245, 2013

Equations (20) and (21) are solved over the stretched grid of Canopy. For our application, it is made of 5 levels with a lowest level at 15 cm above the snowpack. $\tilde{N}_{\mathrm{Surf}}$ and c_{Surf} are taken at the lowest level of Canopy while the net mass flux at the top of Canopy, $F_{\mathrm{Net}\kappa}$, is sent to Meso-NH (Fig. 2).

4 Experimental setup and data

4.1 Case study

We selected and simulated a blowing snow event without concurrent snowfall to propose a first evaluation of Meso-NH/Crocus. It occurred around the experimental site of Col du Lac Blanc, a large north-south oriented pass located at 2720 m a.s.l. close to the Alpe d'Huez ski resort in the French Alps (Fig. 3). Due to the surrounding topography, the pass may be considered as a natural wind tunnel where 90 % of observed wind blows from the north– east or south (Vionnet et al., 2012b).

Intensive measurement campaigns have been performed at the experimental site during winters 2010–2011 and 2011–2012 (Guyomarc'h et al., 2012). They aimed at producing a dataset suitable for the evaluation of blowing snow models in alpine terrain. In-situ measurements were collected during blowing snow events (Fig. 3). They include: (i) meteorological conditions (wind speed and direction, air temperature) at three automatic weather stations (AWS) located around the pass, (ii) vertical profile (up to 3.5 m) of wind speed on a meteorological mast at the pass and (iii) vertical profile of blowing snow fluxes using mechanical snow traps and Snow Particles Counter (SPC, Sato et al., 1993) at the pass. The evolution of snow depth was also followed over an area of 0.54 km^2 around the pass using data from a Terrestrial Laser Scanner (TLS, Prokop, 2008). Overall, six blowing snow events have been investigated during these two winters.

As a case study, we selected a blowing snow event that occurred on 18 and 19 March 2011. Figure 4 describes the meteorological conditions observed at Col du Lac

TCD
7, 2191–2245, 2013

Blanc for this event. 30 cm of fresh snow accumulated with a moderate wind during the night from 16 to 17 March have been redistributed by an intense wind blowing from the North. The blowing snow event started on 18 March at 2 a.m. and lasted until 19 March at 8 a.m. It occurred without snowfall from 18 March at 2 a.m. to 19 March at 3 a.m.

4.2 Coupled model setup

We carried out two simulations for our case study: one with the sublimation of blowing snow (simulation SUBL) and one without (simulation CTRL). Both simulations start on 18 March 1 a.m. and last until 18 March 11 p.m. They cover the period of intense snow transport without concurrent snowfall (Fig. 4).

The simulation domain is centered at Col du Lac Blanc and covered $3 \times 3\,\mathrm{km}^2$ at an horizontal resolution of 50 m (Fig. 3). Meso-NH uses a stretched vertical grid of 70 layers with 20 layers in the lowest 200 m of the atmosphere to reproduce the boundary layer dynamics. The height of the lowest level ranges from 1.9 to 3.1 m due to the terrain-following coordinates. Canopy increases the vertical resolution close to the ground by adding 5 atmospheric layers (lowest level: 15 cm above the snowpack). The snowpack is discretized in Crocus by 20 layers. The value for surface roughness z_0 is based on observations at Col du Lac Blanc (Vionnet, 2012) and is set at 1.3×10^{-4} m. The model time step is 1.5 s.

The Meso-NH model was initialized on 18 March 1 a.m. using a vertical atmospheric sounding. This sounding is first vertically interpolated on the model vertical grid and then distributed homogeneously over the simulation domain. A final adjustment allows the 3-D wind to fulfill the anelastic constraint and the free-slip boundary condition. This final wind field is used as initial field for the Meso-NH model. The vertical sounding is taken from a Meso-NH simulation at an horizontal resolution of 450 m at the grid point corresponding to Col du Lac Blanc. Input and forcing for this simulation come from the analysis of the operational model AROME. Near-surface wind in the sounding is adjusted to match the observed wind field at Col du Lac Blanc. This operation is repeated each hour to produce updated boundary conditions for the atmospheric model.

TCD
7, 2191–2245, 2013

This aims at reproducing the observed temporal evolution of wind speed at Col du Lac Blanc.

The Crocus snowpack model was initialized using an horizontally homogeneous snowpit. 30 cm of erodible snow ($U_{5th} = 9\,m\,s^{-1}$) cover a layer of non-erodible snow as observed at the experimental site before the event. Such method allows to reduce model uncertainties about the initial snowpack but does not reproduce snowpack variability as a function of altitude, slope and aspect.

The current version of the blowing snow scheme requires fixed values for the shape parameter of the Gamma distribution, α, and the average radius of particles in saltation, $r_{m\mathrm{Salt}}$. At Col du Lac, Naaim-Bouvet et al. (2011) have reported values of α ranging from 3 to 4. We took $\alpha = 3$ for the use of Meso-NH/Crocus in alpine terrain. The average radius in the saltation layer has not been measured but values in the suspension layer (between 25 and 29 cm) varies from 65 to 90 µm. Assuming that r_m follows a power law $r_m = az^b$ with $b \approx -0.25$ (Schmidt, 1982), we found values for $r_{m\mathrm{Salt}}$ ranging from 100 to 137 µm. We finally chose $r_{m\mathrm{Salt}} = 110\,\mu m$.

5 Results and discussion

Results of the control simulation CTRL are firstly presented and discussed. The influence of blowing snow sublimation is then considered through a comparison of simulations SUBL and CTRL.

5.1 Atmospheric flow

The most sensitive transport modeling parameter in complex terrain is the driving wind field (e.g. Gauer, 1999; Lehning et al., 2008; Schneiderbauer and Prokop, 2011). In this section, we present an evaluation of the spatial and temporal evolution of the near-surface atmospheric flow simulated by Meso-NH. Figure 5 shows the near-surface

TCD
7, 2191–2245, 2013

modeled wind field at 7 a.m. on 18 March 2011 when maximum wind speed has been measured at Col du Lac Blanc (Fig. 4).

Figure 5 illustrates how topography exerts a strong control on the wind direction and speed. The atmospheric flow is locally channeled along a north–south axis at Col du Lac Blanc (in between AWS Lac Blanc and Muzelle). The presence of ridges modifies also the flow (area A1 and A2 on Fig. 5). Along theses ridges, the wind is normal to the ridge axis while wind speed increases locally. Crest speedup is especially important in area A1 where the near-surface wind speed reaches 33 $m\,s^{-1}$. We believe that the model tends to over-estimate the wind speed in this region. Mott et al. (2010) identified similar over-estimation of crest speed-up in high-resolution (5 m) simulations. They associated it with an insufficient geometrical resolution of sharp crests in the model. Finally, the model simulates the formation of recirculation zone (area R1, R2 and R3 on Fig. 5) in some leeward regions. In these area, the wind direction is variable and may be opposed to the main flow while the wind speed is low. Therefore, Meso-NH is able to reproduce the main characteristics of wind flow in complex terrain (Raderschall et al., 2008): wind channeling, crest speedup and formation of recirculation zone downwind of the ridge. Such small scale flow features are the driving mechanisms behind the inhomogeneous snow distribution resulting from blowing snow events.

Wind speed and directions has been measured at three AWS around Col du Lac Blanc (Fig. 5). Table 2 shows that the model compares relatively well to the observations for the 2 AWS located on both side of the pass (Lac Blanc and Muzelle). Therefore, the radio-sounding method to initialize the atmosphere and to provide lateral boundary conditions allows the model to reproduce the evolution of wind speed at the pass during the blowing snow event. The main flow direction is also satisfactorily reproduced even if the model does not capture the eastern component of the wind at the Lac Blanc AWS. Results are different at the Dome AWS where the model represents well the wind direction but over-estimates the wind speed. At this station, the atmospheric flow is highly turbulent compared to the two other stations. The averaged gust factors (per period of 15 min) measured during the period of intense snow transport (2 a.m. to

TCD
7, 2191–2245, 2013

6 p.m.) are 2.08, 1.31 and 1.35 at AWS Dome, Muzelle and Lac Blanc, respectively. Meso-NH does not represent well this highly turbulent flow and predicts instead a flow with high wind speed. This will influence the intensity of snow redistribution.

The vertical profiles of wind speed close to the surface simulated by the model have been compared to the profiles measured on a 4 m meteorological mast (Fig. 6). For this comparison, measured 15 min mean vertical profiles of wind speed were averaged into four 2 m wind speed bins (1 m s^{-1}) ranging between 13 and 17 m s^{-1}. The same treatment has been applied to simulated profiles. Figure 6 shows that the model reproduces satisfactorily the near-surface vertical profile of wind speed for each category. Canopy turned out to be an adapted tool to refine the vertical profile of wind speed close to the snowpack. This is of prime importance to estimate with accuracy blowing snow fluxes and mass exchanges between the snowpack and the atmosphere.

5.2 Blowing snow fluxes

Meso-NH/Crocus simulates snow transport as a function of the type of surface snow and the wind forcing described at the previous section. Therefore, it is highly variable in space and time. Blowing snow fluxes have been measured at two levels above the surface (1.19 and 3.27 m on average) by two SPCs located at the pass. Fluxes at 1.19 m are roughly one order of magnitude higher than fluxes at 3.27 m (Fig. 7a). A qualitative comparison between modeled and observed fluxes shows that Meso-NH/Crocus captures well the temporal evolution of blowing snow fluxes at both levels. During the period of maximum snow transport (3–7 a.m.), the model is in good agreement with observations at 1.19 m and tends to under-estimate fluxes at 3.27 m. Then, the model reproduces well the decrease of blowing snow fluxes at both levels after 7 a.m. until transport stops at 5 p.m. when the wind speed drops below the threshold wind speed (Fig. 7b). Therefore, the use of Canopy allows to reproduce the strong gradient of blowing snow concentration close to the ground and its evolution during the case study. Meso-NH/Crocus provides a good estimation of the snow mass transported in suspension.

TCD
7, 2191–2245, 2013

5.3 Patterns of snow erosion and deposition

Figure 8 shows how snow has been redistributed in Meso-NH/Crocus during this blowing snow event. We present here a map of difference of snow water equivalent (SWE) which is conserved during snow transport (neglecting sublimation) contrary to snow depth. The model simulates the formation of successive areas of snow erosion and deposition. This map is in agreement with what is qualitatively expected from the wind field structure (Fig. 5). Snow erosion is simulated on windward areas and deposition occurs in regions of decreasing wind speed. Areas of erosion are generally larger than the corresponding areas of deposition.

Maps of snow depth difference measured by TLS measurements have been used in recent studies to evaluate the quality of the snow redistribution simulated by models (Mott et al., 2010; Schneiderbauer and Prokop, 2011). However, this map is not available for our case study. Therefore, instead of a direct comparison, we propose here a qualitative analysis in term of typical patterns of erosion and deposition around Col du Lac Blanc for Northern blowing snow events. We select an event that occurred on 22–26 February 2011 for which TLS data are available. This event presents wind conditions similar to our case study with an averaged wind direction and speed of 24.5° and 11.0 $m\,s^{-1}$ compared to 22.0° and 11.1 $m\,s^{-1}$ for our case study. Note that this comparison cannot be considered as a formal evaluation of the model ability to simulate snow redistribution but aims rather at exploring what is possible with the current model resolution of 50 m.

Figure 9a shows the map of snow depth difference for the event of 22–26 February 2011. This map illustrates the presence of fine scale structures of erosion and deposition. Erosion is mostly observed on the northern side of the pass where area of snow deposition are also present. Their formation is related to topographic features such as cross-loaded slope (arrow 1) and slope change (arrow 2) responsible for the formation of a local recirculation zone on the windward side of the pass. On the southern side, deposition is generally observed with maxima of snow deposition at a steep slope break

TCD
7, 2191–2245, 2013

(arrow 3) and at the bottom of west-facing cliffs (arrow 4). Averaging to an horizontal resolution of 50 m (Fig. 9b) reduces greatly the variability of snow depth difference but keeps general structure of erosion and deposition. Erosion is observed on the northern side of the pass while more located deposition occurred on the southern side.

Figure 9c shows that the model simulated erosion on northern side of the pass and deposition on the southern side for our case study. The location of the main deposition area (arrows 5, 6 and 7) is satisfactorily captured but their extension tends to be overestimated (arrows 5 and 6). The formation of these area of deposition is generated by slope breaks that locally modified the atmospheric flow. A detailed analysis shows that these local topographic features are not present in the 50 m model orography. Therefore, the horizontal resolution of 50 m is not sufficient to reproduce the variability of snow depth difference measured around the pass since erosion and deposition result from small scale flow features generated at scale smaller than 50 m. Mott and Lehning (2010) found similar results at the Gaudergrat ridge (Swiss Alps) where their model at an horizontal resolution of 50 m reproduced patterns of snow deposition at the ridge scale but missed smaller scale deposition patterns. These pattern were partially reproduced using horizontal resolutions of 10 and 5 m. Amory (2012) showed recently that such horizontal resolutions can be achieved with Meso-NH around Col du Lac Blanc but require a large computational effort.

5.4 Influence of blowing snow sublimation

We carried out a second simulation of our case study including blowing snow sublimation (simulation SUBL). A comparison with the reference simulation (simulation CTRL) allows us to discuss the influence of blowing snow sublimation.

As explained in Sect. 3.1.3, blowing snow sublimation acts as a sink of snow mass and modifies in return near-surface meteorological variables. Figure 10 illustrates the effects of blowing snow sublimation on near-surface variables simulated by Meso-NH/Crocus at Col du Lac Blanc. Accounting for sublimation reduces suspended snow concentration of 4 % on average in the first 3 m of the atmosphere. During this event,

TCD
7, 2191–2245, 2013

sublimation rate ranges from 0 to $-2.7\,mm_{SWE}\,day^{-1}$. Such sublimation rates are coherent with results from previous studies. Pomeroy and Essery (1999) measured latent heat fluxes corresponding to sublimation rates ranging from -1.2 to $-1.8\,mm_{SWE}\,day^{-1}$. Combining measurements of vertical profiles of relative humidity and number concentration of particles, Schmidt (1982) found sublimation rates varying between -0.51 et $-5.27\,mm_{SWE}\,day^{-1}$. Figure 10b shows that the sublimation rate is maximal at 7 a.m. when blowing snow concentration reaches its highest value. The evolution of near-surface variables controls also the sublimation rate. For a given snow concentration in the atmosphere, the decrease of humidity at the beginning of the event (3–9 a.m.) changes the sublimation rate. It increases from $-1\,mm_{SWE}\,day^{-1}$ at 4 a.m. to $-2.5\,mm_{SWE}\,day^{-1}$ at 8:20 a.m. for the same snow concentration ($1.5\,g\,m^{-3}$) and a relative humidity dropping from 83 to 58 %.

Sublimation effects on the surface boundary layer are illustrated on Fig. 10c and d. It leads to an increase of relative humidity with respect to ice. It is larger close to the surface with +9.5 % at 0.15 m and +3.6 % at 3.2 m on 18 March at 7 a.m. This increase is smaller than the increase of 15 % simulated by Groot Zwaaftink et al. (2011) for a blowing snow event that occurred in the Swiss Alps. This difference may be explained by drier air in their case study increasing blowing snow sublimation. Nonetheless, our results and those obtained by Groot Zwaaftink et al. (2011) are similar and do not show saturation of the lowest levels of the atmosphere when blowing snow sublimation is activated. The significant increase of relative humidity near the snow surface with blowing snow sublimation mentioned by Déry et al. (1998) is not simulated in 3-D models in alpine terrain. This may be explained by the advection effects included in 3-D models and which are missing in 1-D unless explicitly included like in Bintanja (2001). Blowing snow sublimation affects also potential temperature with a maximum decrease of -0.66 K at 0.15 m. The vertical gradient of potential temperature becomes stronger and increases the stability of the SBL at Col du Lac Blanc.

Blowing snow sublimation reduces snow concentration in the atmosphere and changes in snow redistribution are expected. The difference of SWE at the end of

TCD
7, 2191–2245, 2013

the blowing snow event in simulations SUBL and CTRL is shown on Fig. 11. Blowing snow sublimation reduces snow accumulation in areas of deposition identified on Fig. 8. The averaged deposited snow mass within our model domain is reduced by 5.3 % during this event in simulation SUBL compared to simulation CTRL. This value is slightly higher than the 2.3 % found by Groot Zwaaftink et al. (2011) for a 43 h blowing snow event occurring over an alpine catchment (2.4 km^2) covering the altitude range 1800–2600 m. Other studies focusing on the impact of blowing snow sublimation over a whole winter have found reduction of 4.1 % for the Berchtesgaden park in Germany (210 km^2) (Strasser et al., 2008) and 17 to 19 % along a mountain crest (length: 210 m) in the Canadian Rockies (MacDonald et al., 2010). However, these estimations cannot be directly compared to our results since they have been produced at different spatial scale and cover the whole winter and not a single event like our study.

Figure 11 shows also points where SWE at the end of the event is higher in simulation SUBL than simulation CTRL. To gain understanding on this unexpected increase, we computed the mass balance of a region located on the northern side of Col du Lac Blanc (green box on Fig. 11). It corresponds to an area of snow erosion (Fig. 8). Mean SWE difference between simulations SUBL and CTRL is +0.38 mm. 87 % of this increase is explained by a reduction of erosion flux resulting from a decrease of wind speed associated with higher atmospheric stability. The remaining 13 % are explained by a decrease of surface sublimation in simulation SUBL (cf next paragraph). Therefore, slight modifications of near-surface variables explain the increase of SWE observed at some points at the end of simulation SUBL compared to simulation CTRL.

As mentioned before, accounting for blowing snow sublimation modifies humidity and temperature near the surface and changes eventually turbulent fluxes between the snowpack and the atmosphere. The detailed mass balance of a deposition area (Table 3) shows that the increase of relative humidity reduces surface sublimation by 29.7 %. Such reduction has been observed by Wever et al. (2009) in wind tunnel experiments. Bintanja (2001) even suggested that the total sublimation (surface+blowing snow) could be smaller than surface sublimation without snow transport due to the

TCD
7, 2191–2245, 2013

self-regulation of blowing snow sublimation (Déry et al., 1998). For our case study, Meso-NH/Crocus simulates total sublimation loss of 1.46 mm for simulation SUBL and 0.47 mm for simulation CTRL. Therefore, for this case study and for the selected deposition area, the total sublimation is multiplied by 3 when accounting for blowing snow sublimation which becomes the main source of transfer of water vapor to the atmosphere (78 % of total sublimation).

The computation of blowing snow sublimation in Meso-NH/Crocus has several limitations. Firstly, the model assumes that the ventilation velocity is equal to the settling velocity of suspended particles and neglects ventilation effects associated to turbulence (Dover, 1993; Bintanja, 2000). Furthermore, the effect of solar radiation is not included in the computation of the sublimation rate of an ice sphere. Measurements in wind-tunnel (Wever et al., 2009) show that solar radiation may increase sublimation by 50 %. Finally, our model assumes that suspended snow particles are spherical. Based on the results of Thorpe and Mason (1966), Wever et al. (2009) estimated that the efficiency of the mass and energy exchange increased a factor 2.5 to 5 for dendritic shapes compared to hexagonal plates. The highest sublimation rates are observed with crystals composed of very fine branches. We estimate this effect is only active at the onset of blowing snow events before fragmentation modifies particles shape towards more rounded particles (Clifton et al., 2006; Vionnet et al., 2012b). All these limitations lead to a probable under-estimation of blowing snow sublimation rates by the model.

6 Conclusions

In this paper, we have introduced the coupled system Meso-NH/Crocus dedicated to the study of snowpack/atmosphere interactions and wind-induced snow redistribution during blowing snow events. It includes a blowing snow scheme which makes the distinction between snow transport in saltation and turbulent suspension. In the atmosphere, blown snow particles are represented by a double moment scheme to capture the spatial and temporal evolution of the particle size distribution. At the surface,

TCD
7, 2191–2245, 2013

the model computes mass flux in saltation as a function of snow-surfaces properties given by Crocus and near-surface meteorological conditions. The resulting snow erosion or deposition includes the contributions of snow transport in saltation and turbulent suspension, and snowfall simulated by Meso-NH. The use of a SBL scheme at the interface between Crocus and Meso-NH increases the vertical resolution close to the ground to reproduce strong gradients of blowing snow concentration and compute mass exchanges between the snowpack and the atmosphere.

The results of Meso-NH/Crocus in alpine terrain were evaluated for a 22 h blowing snow event observed around the experimental site of Col du Lac Blanc (2720 m a.s.l, French Alps). It occurred without concurrent snowfall. At an horizontal resolution of 50 m, Meso-NH is able to capture the main features of near-surface atmospheric flow in alpine terrain including crest speed-up and the formation of recirculation zones. It also reproduced satisfactorily the vertical profile of wind speed and of blowing snow fluxes near the surface. The resulting area of erosion and deposition are in agreement with what is qualitatively expected from the wind field structure: snow erosion on windward areas and deposition in regions of decreasing wind speed. However, the resolution of 50 m is not sufficient to reproduce the extension of these area around Col du Lac Blanc compared to measurements from terrestrial laser scanner. Their formation is indeed governed by topographic features of scale lower than 50 m.

Blowing snow sublimation is implemented in the coupled model which accounts for feedback on the near-surface variables (humidity, temperature). When activated for this case study, blowing snow sublimation reduces by 5 % the total amount of deposited snow. It modifies also the surface boundary layer in regions exposed to drifting snow and downwind of these zones with an increase of relative humidity by 5 to 9 % and a decrease of potential temperature by 0.3 to 0.7 K. Advection effects prevent from the formation of a near-surface saturated layer. During this blowing snow event, blowing snow sublimation is the main source of water vapor transfer to the atmosphere and represents 78 % of total sublimation (blowing snow + surface).

TCD
7, 2191–2245, 2013

Several simplifications and limitations of the model formulation have been identified through this first evaluation. The adaptation to snow of the formulation of Sørensen (2004) for the saltation mass flux presents some limitations. It must be adjusted and eventually be replaced by a physically-based saltation model (e.g. Kok and Renno, 2009). The description of mechanical transformation of snow grain under transport is still poor and will require developments similar to those implemented in the model of Durand et al. (2005). The spherical assumption for blown snow particles is also questionable and has an impact on the aerodynamic properties of suspended particles. Finally, limitations concerning blowing snow sublimation have been discussed.

Future developments will include the simulation of blowing snow events at higher horizontal resolution (up to 10 m) around Col du Lac Blanc to allow direct comparison with measurement from terrestrial laser scanner. This will be made possible by the on-going development of more efficient numerical schemes in Meso-NH. A second application concerns the simulation of blowing snow events with concurrent snowfall which represent 37 % of observed blowing snow events at Col du Lac Blanc (Vionnet et al., 2012b). The explicit representation of snowfall and blowing snow in the model will allow us to study the relative contribution of ground snow transport and preferential deposition of snowfall (Lehning et al., 2008; Dadic et al., 2010) to the spatial variability of the snowpack. This will require the use of grid-nesting techniques to produce atmospheric forcing from the synoptic scale down to the local scale.

Meso-NH/Crocus is the first fully couped snowpack/atmosphere model which can simulate wind-induced snow transport at high-resolution in alpine terrain. It can be also applied over other snow-covered terrain such as regions of Antarctica (Gallée et al., 2013) or over glaciers (Sauter et al., 2013). Its applications can be also extended to other topics regarding snowpack/atmosphere interactions such as the dynamics of katabatic wind over glacier (e.g. Claremar et al., 2012) or the influence of a patchy snow cover on the dynamics of the SBL (Mott et al., 2012).

TCD
7, 2191–2245, 2013

Appendix A

Symbols and units.

Symbol	Units	Description
C_D	(–)	Transfer coefficient for momentum
D_v	$m^2 s^{-1}$	Molecular diffusivity of water vapor
F_{Net}	$kg m^{-2} s^{-1}$	Net mass flux between the snowpack and the atmosphere
F_{Precip}	$kg m^{-2} s^{-1}$	Snowfall rate
F_{Salt}	$kg m^{-2} s^{-1}$	Contribution to F_{Net} of snow transport in saltation
F_{Susp}	$kg m^{-2} s^{-1}$	Contribution to F_{Net} of snow transport in turbulent suspension
K_{air}	$J m^{-1} s^{-1} K^{-1}$	Molecular thermal conductivity of the air
K_{Sca}	$m^2 s^{-1}$	Coefficient of turbulent diffusion for passive scalar in Meso-NH
K_{Snw}	$m^2 s^{-1}$	Coefficient of turbulent diffusion for blowing snow variables
L_m	m	Mixing length
L_s	$J kg^{-1}$	Latent heat of sublimation for ice
N_s	kg^{-1}	Number concentration of particles per unit of mass
$\tilde{N}_{Salt}$	m^{-3}	Number concentration per unit of volume at the top of the saltation layer
$\tilde{N}_{Surf}$	m^{-3}	Number concentration per unit of volume at the bottom of Canopy
Nu	(–)	Nusselt number
P_{air}	Pa	Air pressure
Q_{Salt}	$kg m^{-1} s^{-1}$	Horizontal transport rate in saltation
Re	(–)	Particle Reynods number
R_v	$J kg^{-1} K^{-1}$	Specific constant for water vapor
Sh	(–)	Sherwood number
SWE	$kg m^{-2}$	Snow water equivalent
S_N	$kg^{-1} s^{-1}$	Number sublimation rate
S_q	$kg kg^{-1} s^{-1}$	Mass sublimation rate
T_{air}	K	Air temperature
U_{Surf}	$m s^{-1}$	Wind speed at the bottom of Canopy

TCD
7, 2191–2245, 2013

Symbol	Units	Description
U_{xt}	$m\,s^{-1}$	Threshold wind speed at x m
U_x	$m\,s^{-1}$	Wind speed at x m
V_N	$m\,s^{-1}$	Number-weighted mean particle fall speed
V_q	$m\,s^{-1}$	Mass-weighted mean particle fall speed
V_v	$m\,s^{-1}$	Ventilation speed
c_{Salt}	$kg\,m^{-3}$	Snow mass concentration in the saltation layer
c_{Surf}	$kg\,m^{-3}$	Blowing snow mass concentration at the bottom of Canopy
e	Pa	Vapor pressure
e_{si}	Pa	Vapor pressure at saturation over ice
e_{TKE}	$m^2\,s^{-2}$	Kinetic turbulent energy
g	$m\,s^{-2}$	Acceleration due to gravity
h_{Salt}	m	Thickness of the saltation layer
q_s	$kg\,kg^{-1}$	Blowing snow mixing ratio
r	m	Particle radius
r_m	m	Mean particle radius
r_{msalt}	m	Mean particle radius in the saltation layer
u_{part}	$m\,s^{-1}$	Particle speed in the saltation layer
u_j	$m\,s^{-1}$	Wind speed in direction j
u_*	$m\,s^{-1}$	Friction velocity
u_{*t}	$m\,s^{-1}$	Threshold friction velocity
z_0	m	Roughness length
Γ	(–)	Gamma function
α	(–)	Shape parameter of the gamma law
β	m	Scale parameter of the gamma law
ζ	(–)	K_{Sca}/K_{Snw}
ν_{air}	$m^2\,s^{-1}$	Air kinematic viscosity
ρ_{air}	$kg\,m^{-3}$	Air density
ρ_{ice}	$kg\,m^{-3}$	Ice density
σ	(–)	Water vapor deficit with respect to ice (= $(e - e_{si})/e_{si}$)

TCD
7, 2191–2245, 2013

Appendix B

Advection of blowing snow variables in Canopy

A Canopy is a 1-D SBL scheme included in SURFEX (Masson and Seity, 2009). Blowing snow variables have been introduced in this scheme to reproduce the strong gradient of blowing snow concentration close to the ground. The contribution of advection at each Canopy levels is included through specific terms appearing in Eqs. (20) and (21). We detailed here the calculation steps for the blowing mixing ratio, q_s (written q in the following). The same method is used for the number concentration per unit of mass, N_s. The procedure follows :

1. The total mass flux in Canopy ($\mathrm{kg\,m^{-1}\,s^{-1}}$) is computed following $Q_{\mathrm{Cano}} = \rho_{\mathrm{air}} \sum_i q_i h_i u_i$ where h_i is the thickness of Canopy layer i and u_i the wind speed at level i.

2. An equivalent concentration is deduced from $c_{\mathrm{eq}} = Q_{\mathrm{Cano}}/(h_{\mathrm{MNH}} u_{\mathrm{MNH}})$ ($\mathrm{kg\,m^{-3}}$) where h_{MNH} is the thickness of the first atmospheric layer and u_{MNH} the wind speed at the first level of Meso-NH.

3. Meso-NH computes the advection at the first atmospheric layer of the field $r_{\mathrm{eq}} = c_{\mathrm{eq}}/\rho_a$ and sends back to Canopy the advected variable c_{adv}.

4. The total snow mass in Canopy M_{Cano} ($= \rho_{\mathrm{air}} \sum_i q_i h_i$) is updated following: $M'_{\mathrm{Cano}} = M_{\mathrm{Cano}} + M_{\mathrm{adv}} - M_{\mathrm{eq}}$ where $M_{\mathrm{adv}} = c_{\mathrm{adv}}/h_{\mathrm{MNH}}$ et $M_{\mathrm{eq}} = c_{\mathrm{eq}}/h_{\mathrm{MNH}}$.

5. The contribution of advection at each level i is finally computed as:

$$\left(\frac{\partial q_i}{\partial t}\right)_{\mathrm{Adv}} = M'_{\mathrm{Cano}}/M_{\mathrm{Cano}} - 1 \qquad \text{(B1)}$$

TCD
7, 2191–2245, 2013

Acknowledgements. We thank Ph. Puglièse and H. Bellot for support at Col du Lac Blanc and S. Faroux, G. Tanguy and J. Payart for technical help with SURFEX and Meso-NH. We also thank E. Brun for many meaningful scientific discussions. This work, including the field campaign, has been partially supported by the French INSU LEFE/IDAO programme under the INEV project and the French-Austrian cooperation program AMADEUS.

The publication of this article is financed by CNRS-INSU.

References

Amory, C.: Simulation numérique à haute résolution du champ de vent en couche limite atmosphérique sur relief complexe. Application à un site d'étude du transport de neige par le vent: le Col du Lac Blanc (Alpe d'Huez, France), Master's thesis, Laboratoire des Ecoulements Géophysiques et Industriels, Université Joseph Fourier, Grenoble, France, 2012, in French. 2214

Aumond, P., Masson, V., Lac, C., Gauvreau, B., Dupont, S., and Berengier, M.: Including the drag effects of canopies: real case large-eddy simulation studies, Bound.-Lay. Meteorol., 146, 1–16, 2012. 2206

Beffrey, G., Jaubert, G., and Dabas, A.: Foehn flow and stable air mass in the Rhine valley: the beginning of a MAP event, Q. J. Roy. Meteor. Soc., 130, 541–560, 2004. 2196

Bernhardt, M., Zängl, G., Liston, G., Strasser, U., and Mauser, W.: Using wind fields from a high-resolution atmospheric model for simulating snow dynamics in mountainous terrain, Hydrol. Process., 23, 1064–1075, 2009. 2194

Bernhardt, M., Liston, G. E., Strasser, U., Zängl, G., and Schulz, K.: High resolution modelling of snow transport in complex terrain using downscaled MM5 wind fields, The Cryosphere, 4, 99–113, doi:10.5194/tc-4-99-2010, 2010. 2194

TCD

7, 2191–2245, 2013

Bintanja, R.: Snowdrift suspension and atmospheric turbulence. Part I: Theoretical background and model description, Bound.-Lay. Meteorol., 95, 343–368, 2000. 2198, 2201, 2202, 2203, 2217

Bintanja, R.: Modelling snowdrift sublimation and its effect on the moisture budget of the atmospheric boundary layer, Tellus A, 53, 215–232, 2001. 2215, 2216

Bougeault, P., Binder, P., Buzzi, A., Dirks, R., Houze, R., Kuettner, J., Smith, R., Steinacker, R., and Volkert, H.: The MAP special observing period, B. Am. Meteorol. Soc., 82, 433–462, 2001. 2196

Brun, C. and Chollet, J.: LES of Scalar transport in a turbulent katabatic flow along a curved slope in the context of stably stratified atmospheric boundary layer, in: Proceedings of the EGU General Assembly, 2–7 May, 2010, Vienna, Austria, 2010. 2196

Brun, E., Martin, E., Simon, V., Gendre, C., and Coleou, C.: An energy and mass balance model of snow cover suitable for operational avalanche forecasting, J. Glaciol., 35, 333–342, 1989. 2196

Brun, E., David, P., Sudul, M., and Brunot, G.: A numerical model to simulate snow cover stratigraphy for operational avalanche forecasting, J. Glaciol., 38, 13–22, 1992. 2196

Budd, W.: The drifting of non-uniform snow particles, Studies in Antarctic Meteorology, 9, 1966. 2198, 2206

Carpenter, R., Droegemeier, K., Woodward, P., and Hane, C.: Application of the piecewise parabolic method (PPM) to meteorological modeling, Mon. Weather Rev., 118, 586–612, 1990. 2199

Carrier, C.: On Slow Viscous Flow, Tech. rep., Office of Naval Research, Contract Nonr-653(00), Brown University, Providence, RI, 1953. 2201

Claremar, B., Obleitner, F., Reijmer, C., Pohjola, V., Waxegård, A., Karner, F., and Rutgersson, A.: Applying a mesoscale atmospheric model to Svalbard Glaciers, Adv. Meteorol., 2012, 321649, doi:10.1155/2012/321649, 2012. 2219

Clifton, A., Ruedi, J., and Lehning, M.: Snow saltation threshold measurements in a drifting-snow wind tunnel, J. Glaciol., 52, 585–596, 2006. 2217

Colella, P. and Woodward, P.: The piecewise parabolic method (PPM) for gas-dynamical simulations, J. Comput. Phys., 54, 174–201, 1984. 2199

Cuxart, J., Bougeault, P., and Redelsperger, J.: A turbulence scheme allowing for mesoscale and large-eddy simulations, Q. J. Roy. Meteor. Soc., 126, 1–30, 2000. 2196, 2199

TCD
7, 2191–2245, 2013

Dadic, R., Mott, R., Lehning, M., and Burlando, P.: Wind influence on snow depth distribution and accumulation over glaciers, J. Geophys. Res., 115, F01012, doi:10.1029/2009JF001261, 2010. 2195, 2219
Deardorff, J.: Numerical investigation of neutral and unstable planetary boundary layers, J. Atmos. Sci., 29, 91–115, 1972. 2200
Déry, S. and Yau, M.: A bulk blowing snow model, Bound.-Lay. Meteorol., 93, 237–251, 1999. 2202
Déry, S. and Yau, M.: Simulation of blowing snow in the Canadian Arctic using a double-moment model, Bound.-Lay. Meteorol., 99, 297–316, 2001a. 2198, 2202
Déry, S. and Yau, M.: Simulation of an Arctic ground blizzard using a coupled blowing snow-atmosphere model, J. Hydrometeorol., 2, 579–598, 2001b. 2194
Déry, S., Taylor, P., and Xiao, J.: The thermodynamic effects of sublimating, blowing snow in the atmospheric boundary layer, Bound.-Lay. Meteorol., 89, 251–283, 1998. 2193, 2201, 2202, 2215, 2217
Doorschot, J. and Lehning, M.: Equilibrium saltation: mass fluxes, aerodynamic entrainment, and dependence on grain properties, Bound.-Lay. Meteorol., 104, 111–130, 2002. 2204
Dover, S.: Numerical Modelling of Blowing Snow, Ph.D. thesis, University of Leeds, UK, 1993. 2198, 2200, 2202, 2217
Durand, Y., Brun, E., Mérindol, L., Guyomarc'h, G., Lesaffre, B., and Martin, E.: A meteorological estimation of relevant parameters for snow models, Ann. Glaciol., 18, 65–71, 1993. 2238
Durand, Y., Giraud, G., Brun, E., Mérindol, L., and Martin, E.: A computer-based system simulating snowpack structures as a tool for regional avalanche forecasting, J. Glaciol., 45, 469–484, 1999. 2197
Durand, Y., Guyomarc'h, G., and Merindol, L.: Numerical experiments of wind transport over a mountainous instrumented site: I. Regional scale, Ann. Glaciol., 32, 187–194, 2001. 2197
Durand, Y., Guyomarc'h, G., Mérindol, L., and Corripio, J.: Improvement of a numerical snow drift model and field validation, Cold Reg. Sci. Technol., 43, 93–103, 2005. 2192, 2193, 2197, 2203, 2219
Föhn, P.: Snow transport over mountain crests, J. Glaciol., 26, 469–480, 1980. 2192
Gallée, H., Guyomarc'h, G., and Brun, E.: Impact of snow drift on the Antarctic ice sheet surface mass balance: possible sensitivity to snow-surface properties, Bound.-Lay. Meteorol., 99, 1–19, 2001. 2194, 2199, 2203, 2206

TCD
7, 2191–2245, 2013

Gallée, H., Trouvilliez, A., Agosta, C., Genthon, C., Favier, V., and Naaim-Bouvet, F.: Transport of snow by the wind: a comparison between observations in Adélie Land, Antarctica, and simulations made with the regional climate model MAR, Bound.-Lay. Meteorol., 146, 1–15, 2013. 2219

Gauer, P.: Blowing and drifting snow in Alpine terrain: a physically-based numerical model and related field measurements, Ph.D. thesis, Swiss Federal Institute of Technology, Zürich, 1999. 2193, 2194, 2197, 2205, 2210

Gordon, M. and Taylor, P.: Measurements of blowing snow, Part I: Particle shape, size distribution, velocity, and number flux at Churchill, Manitoba, Canada, Cold Reg. Sci. Technol., 55, 63–74, 2009. 2198, 2206

Grell, G., Dudhia, J., and Stauffer, D.: A description of the fifth-generation Penn State/NCAR Mesoscale Model (MM5), NCAR Tech. Note TN-398+ STR, 122, 1995. 2194

Groot Zwaaftink, C., Löwe, H., Mott, R., Bavay, M., and Lehning, M.: Drifting snow sublimation: a high-resolution 3-D model with temperature and moisture feedbacks, J. Geophys. Res., 116, D16107, doi:10.1029/2011JD015754, 2011. 2193, 2195, 2201, 2202, 2215, 2216

Guyomarc'h, G. and Mérindol, L.: Validation of an application for forecasting blowing snow, Ann. Glaciol., 26, 138–143, 1998. 2193, 2203

Guyomarc'h, G., Durand, Y., and Giraud, G.: Towards an integration of snowdrift modeling in the opearational avalanche forecsast, in: Proceedings of the International Snow Science Workshop, Whistler, Canada, 642–648, 2008. 2192

Guyomarc'h, G., Bellot, H., Durand, Y., Naaim-Bouvet, F., Prokop, A., and Vionnet, V.: Measurement campaigns to investigate blowing snow and snow drift conditions at a high altitude site, in: Proceedings, 2012 International Snow Science Workshop, Anchorage, Alaska, 2012. 2208

Kok, J. and Renno, N.: A comprehensive numerical model of steady state saltation (COMSALT), J. Geophys. Res., 114, D17204, doi:10.1029/2009JD011702, 2009. 2219

Kosugi, K., Nishimura, K., and Maeno, N.: Snow ripples and their contribution to the mass transport of drifting snow, Bound.-Lay. Meteorol., 59, 59–66, 1992. 2193

Lafore, J. P., Stein, J., Asencio, N., Bougeault, P., Ducrocq, V., Duron, J., Fischer, C., Héreil, P., Mascart, P., Masson, V., Pinty, J. P., Redelsperger, J. L., Richard, E., and Vilà-Guerau de Arellano, J.: The Meso-NH Atmospheric Simulation System. Part I: adiabatic formulation and control simulations, Ann. Geophys., 16, 90–109, doi:10.1007/s00585-997-0090-6, 1998. 2196

TCD
7, 2191–2245, 2013

Lascaux, F., Richard, E., and Pinty, J.: Numerical simulations of three different MAP IOPs and the associated microphysical processes, Q. J. Roy. Meteor. Soc., 132, 1907–1926, 2006. 2196
Lee, L.: Sublimation of snow in turbulent atmosphere, Ph.D. thesis, University of Wyoming, 1975. 2202
Lehning, M., Doorschot, J., and Bartelt, P.: A snowdrift index based on SNOWPACK model calculations, Ann. Glaciol., 31, 382–386, 2000. 2193
Lehning, M., Löwe, H., Ryser, M., and Raderschall, N.: Inhomogeneous precipitation distribution and snow transport in steep terrain, Water Resour. Res., 44, W07404, doi:10.1029/2007WR006545, 2008. 2193, 2194, 2195, 2197, 2204, 2205, 2210, 2219
Lenaerts, J., van den Broeke, M., Déry, S., van Meijgaard, E., van de Berg, W., Palm, S., and Rodrigo, J.: Modeling drifting snow in Antarctica with a regional climate model: 1. Methods and model evaluation, J. Geophys. Res., 117, D05108, doi:10.1029/2011JD016145, 2012. 2194
Liston, G. and Sturm, M.: A snow-transport model for complex terrain, J. Glaciol., 44, 498–516, 1998. 2201
Liston, G., Haehnel, R., Sturm, M., Hiemstra, C., Berezovskaya, S., and Tabler, R.: Simulating complex snow distributions in windy environments using SnowTran-3D, J. Glaciol., 53, 241–256, 2007. 2193, 2194, 2197
Liu, Y., Warner, T., Liu, Y., Vincent, C., Wu, W., Mahoney, B., Swerdlin, S., Parks, K., and Boehnert, J.: Simultaneous nested modeling from the synoptic scale to the LES scale for wind energy applications, J. Wind Eng. Ind. Aerod., 99, 308–319, 2011. 2195
Louis, J.: A parametric model of vertical eddy fluxes in the atmosphere, Bound.-Lay. Meteorol., 17, 187–202, 1979. 2203
MacDonald, M. K., Pomeroy, J. W., and Pietroniro, A.: On the importance of sublimation to an alpine snow mass balance in the Canadian Rocky Mountains, Hydrol. Earth Syst. Sci., 14, 1401–1415, doi:10.5194/hess-14-1401-2010, 2010. 2193, 2195, 2216
Mann, G.: Surface Heat and water vapour budgets over Antarctica, Ph.D. thesis, The Environment Center, The University of Leeds, UK, 1998. 2198, 2206
Masson, V. and Seity, Y.: Including atmospheric layers in vegetation and urban offline surface schemes, J. Appl. Meteorol. Clim., 48, 1377–1397, 2009. 2197, 2207
Masson, V., Le Moigne, P., Martin, E., Faroux, S., Alias, A., Alkama, R., Belamari, S., Barbu, A., Boone, A., Bouyssel, F., Brousseau, P., Brun, E., Calvet, J.-C., Carrer, D., Decharme, B.,

TCD
7, 2191–2245, 2013

Delire, C., Donier, S., Essaouini, K., Gibelin, A.-L., Giordani, H., Habets, F., Jidane, M., Kerdraon, G., Kourzeneva, E., Lafaysse, M., Lafont, S., Lebeaupin Brossier, C., Lemonsu, A., Mahfouf, J.-F., Marguinaud, P., Mokhtari, M., Morin, S., Pigeon, G., Salgado, R., Seity, Y., Taillefer, F., Tanguy, G., Tulet, P., Vincendon, B., Vionnet, V., and Voldoire, A.: The SURFEXv7.2 land and ocean surface platform for coupled or offline simulation of Earth surface variables and fluxes, Geosci. Model Dev. Discuss., 5, 3771–3851, doi:10.5194/gmdd-5-3771-2012, 2012. 2196

Meister, R.: Influence of strong winds on snow distribution and avalanche activity, Ann. Glaciol., 13, 195–201, 1989. 2193

Michioka, T. and Chow, F.: High-resolution large-eddy simulations of scalar transport in atmospheric boundary layer flow over complex terrain, J. Appl. Meteorol. Clim., 47, 3150–3169, 2008. 2194

Mott, R. and Lehning, M.: Meteorological modeling of very high-resolution wind fields and snow deposition for mountains, J. Hydrometeorol., 11, 934–949, 2010. 2194, 2214

Mott, R., Schirmer, M., Bavay, M., Grünewald, T., and Lehning, M.: Understanding snow-transport processes shaping the mountain snow-cover, The Cryosphere, 4, 545–559, doi:10.5194/tc-4-545-2010, 2010. 2192, 2194, 2195, 2204, 2211, 2213

Mott, R., Gromke, C., Grünewald, T., and Lehning, M.: Relative importance of advective heat transport and boundary layer decoupling in the melt dynamics of a patchy snow cover, Adv. Water Resour., 55, 88–97, doi:10.1016/j.advwatres.2012.03.001, 2012. 2219

Naaim, M., Naaim-Bouvet, F., and Martinez, H.: Numerical simulation of drifting snow: erosion and deposition models, Ann. Glaciol., 26, 191–196, 1998. 2193

Naaim-Bouvet, F., Naaim, M., Bellot, H., and Nishimura, K.: Wind and drifting-snow gust factor in an Alpine context, Ann. Glaciol., 52, 223–230, 2011. 2198, 2210

Nemoto, M. and Nishimura, K.: Numerical simulation of snow saltation and suspension in a turbulent boundary layer, J. Geophys. Res., 109, D18206, doi:10.1029/2004JD004657, 2004. 2204

Nishimura, K. and Hunt, J.: Saltation and incipient suspension above a flat particle bed below a turbulent boundary layer, J. Fluid Mech., 417, 77–102, 2000. 2204

Nishimura, K. and Nemoto, M.: Blowing snow at Mizuho station, Antarctica, Philos. T. R. Soc. A, 363, 1647–1662, 2005. 2198, 2199

Noilhan, J. and Planton, S.: A simple parameterization of land surfaces processes for meteorological models, Mon. Weather Rev., 117, 536–549, 1989. 2196

TCD
7, 2191–2245, 2013

Pinty, J. and Jabouille, P.: A mixed-phase cloud parameterization for use in a mesoscale non-hydrostatic model: simulations of a squall line and of orographic precipitations, in: Conf. on Cloud Physics, 217–220, 1998. 2196, 2199, 2205
Pomeroy, J. and Essery, R.: Turbulent fluxes during blowing snow: field tests of model sublimation predictions, Hydrol. Process., 13, 2963–2975, 1999. 2215
Pomeroy, J. and Gray, D.: Saltation of snow, Water Resour. Res, 26, 1583–1594, 1990. 2204
Pomeroy, J. and Male, D.: Steady-state suspension of snow, J. Hydrol., 136, 275–301, 1992. 2204
Prokop, A.: Assessing the applicability of terrestrial laser scanning for spatial snow depth measurements, Cold Reg. Sci. Technol., 54, 155–163, 2008. 2208
Pruppacher, H., Klett, J., and Wang, P.: Microphysics of Clouds and Precipitation, 1998. 2202
Raderschall, N., Lehning, M., and Schär, C.: Fine-scale modeling of the boundary layer wind field over steep topography, Water Resour. Res., 44, W09425, doi:10.1029/2007WR006544, 2008. 2211
Redelsperger, J. and Sommeria, G.: Méthode de représentation de la turbulence d'échelle inférieure à la maille pour un modèle tri-dimensionnel de convection nuageuse, Bound.-Lay. Meteorol., 21, 509–530, 1981. 2200
Redelsperger, J., Mahé, F., and Carlotti, P.: A simple and general subgrid model suitable both for surface layer and free-stream turbulence, Bound.-Lay. Meteorol., 101, 375–408, 2001. 2200
Sato, T., Kimura, T., Ishimaru, T., and Maruyama, T.: Field test of a new snow-particle counter (SPC) system, Ann. Glaciol., 18, 149–154, 1993. 2208
Sauter, T., Möller, M., Finkelnburg, R., Grabiec, M., Scherer, D., and Schneider, C.: Snowdrift modelling for Vestfonna ice cap, north-eastern Svalbard, The Cryosphere Discuss., 7, 709–741, doi:10.5194/tcd-7-709-2013, 2013. 2219
Schmidt, R.: Threshold wind-speeds and elastic impact in snow transport, J. Glaciol., 26, 453–467, 1980. 2193
Schmidt, R.: Vertical profiles of wind speed, snow concentrations, and humidity in blowing snow, Bound.-Lay. Meteorol., 23, 223–246, 1982. 2193, 2202, 2210, 2215
Schneiderbauer, S. and Prokop, A.: The atmospheric snow-transport model: SnowDrift3D, J. Glaciol., 57, 526–542, 2011. 2193, 2194, 2210, 2213
Schweizer, J., Jamieson, J. B., and Schneebeli, M.: Snow avalanche formation, Rev. Geophys., 41, 1016, doi:10.1029/2002RG000123, 2003. 2192

TCD
7, 2191–2245, 2013

Skamarock, W.: Positive-definite and monotonic limiters for unrestricted-time-step transport schemes, Mon. Weather Rev., 134, 2241–2250, 2006. 2199
Sørensen, M.: An analytic model of wind-blown sand transport, Acta Mech., 1 (Suppl.), 67–81, 1991. 2204
Sørensen, M.: On the rate of aeolian sand transport, Geomorphology, 59, 53–62, 2004. 2203, 2219
Stein, J.: Exploration of some convective regimes over the Alpine orography, Q. J. Roy. Meteor. Soc., 130, 481–502, 2004. 2196
Strasser, U., Bernhardt, M., Weber, M., Liston, G. E., and Mauser, W.: Is snow sublimation important in the alpine water balance?, The Cryosphere, 2, 53–66, doi:10.5194/tc-2-53-2008, 2008. 2193, 2195, 2216
Talbot, C., Bou-Zeid, E., and Smith, J.: Nested mesoscale large-Eddy simulations with WRF: performance in real test cases, J. Hydrometeorol., 13, 1421–1441, 2012. 2195
Thorpe, A. and Mason, B.: The evaporation of ice spheres and ice crystals, Brit. J. Appl. Phys., 17, 541, doi:10.1088/0508-3443/17/4/316, 1966. 2201, 2217
Vionnet, V.: Etudes du transport de la neige par le vent en conditions alpines: observations et simulation à l'aide d'un modèle couplé atmosphère/manteau neigeux, Ph.D. thesis, Sciences et Techniques de l'Envitonnement, Université Paris-Est, France, available at: http://tel.archives-ouvertes.fr/tel-00781279, 2012. 2200, 2209
Vionnet, V., Brun, E., Morin, S., Boone, A., Faroux, S., Le Moigne, P., Martin, E., and Willemet, J.-M.: The detailed snowpack scheme Crocus and its implementation in SURFEX v7.2, Geosci. Model Dev., 5, 773–791, doi:10.5194/gmd-5-773-2012, 2012a. 2196, 2197
Vionnet, V., Guyomarc'h, G., Naaim Bouvet, F., Martin, E., Durand, Y., Bellot, H., Bel, C., and Puglièse, P.: Occurrence of blowing snow events at an alpine site over a 10-year period: observations and modelling, Adv. Water Resour., 55, 53–63, doi:10.1016/j.advwatres.2012.05.004, 2012b. 2203, 2208, 2217, 2219
Weigel, A., Chow, F., Rotach, M., Street, R., and Xue, M.: High-resolution large-eddy simulations of flow in a steep Alpine valley. Part II: Flow structure and heat budgets, J. Appl. Meteorol. Clim., 45, 87–107, 2006. 2194
Wever, N., Lehning, M., Clifton, A., Rüedi, J., Nishimura, K., Nemoto, M., Yamaguchi, S., and Sato, A.: Verification of moisture budgets during drifting snow conditions in a cold wind tunnel, Water Resour. Res, 45, W07423, doi:10.1029/2008WR007522, 2009. 2201, 2216, 2217

TCD
7, 2191–2245, 2013

Xue, M., Droegemeier, K., and Wong, V.: The Advanced Regional Prediction System (ARPS) – a multi-scale nonhydrostatic atmospheric simulation and prediction model. Part I: Model dynamics and verification, Meteorol. Atmos. Phys., 75, 161–193, 2000. 2194

Yang, J. and Yau, M.: A new triple-moment blowing snow model, Bound.-Lay. Meteorol., 126, 137–155, 2008. 2198

TCD

7, 2191–2245, 2013

Table 1. Characteristics of deposited snow resulting from snow transport.

Variable	Density	Dendricity	Sphericity
Unit	kg m^{-3}	(–)	(–)
Value	250	0.3	0.85

TCD
7, 2191–2245, 2013

Table 2. Root mean square error (RMSE) and bias for wind speed, U, and direction, Dir, between simulation CTRL and measurements at three AWS located around Col du Lac Blanc (Fig. 5). Modeled wind speed was scaled to measurement height of AWS assuming a logarithmic wind profile.

	U ($m s^{-1}$)		Dir (°)	
Station	RMSE	Bias	RMSE	Bias
Lac Blanc	1.23	0.42	17.30	−13.88
Muzelle	1.31	−0.35	9.58	1.61
Dome	7.50	6.67	13.63	5.30

TCD
7, 2191–2245, 2013

Table 3. Mass balance (in mm_{SWE}) of a deposition area located on the southern side of Col du Lac Blanc for the case study. Its location is given on Fig. 11. A positive value indicates accumulation. Bold values refers to relative difference in % compared to simulation CTRL.

Simulation	Blowing snow deposition	Surface sublimation	Total
CTRL	+19.99	−0.47	+19.52
SUBL	+18.86	−0.33	+18.53
SUBL-CTRL	−1.13 (−**5.7**%)	+0.14 (+**29.7**%)	−0.99 (−**5.1**%)

TCD
7, 2191–2245, 2013

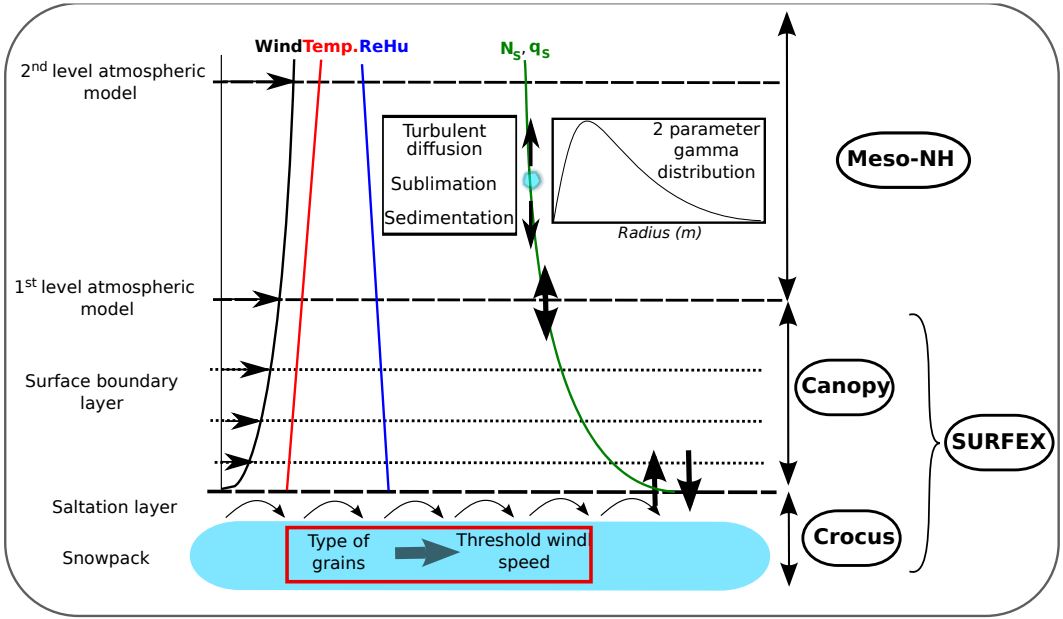

Fig. 1. Components of the blowing snow scheme in Meso-NH/Crocus. N_s denotes the number concentration per unit of mass of blown snow particles and q_s the blowing snow mixing ratio.

TCD
7, 2191–2245, 2013

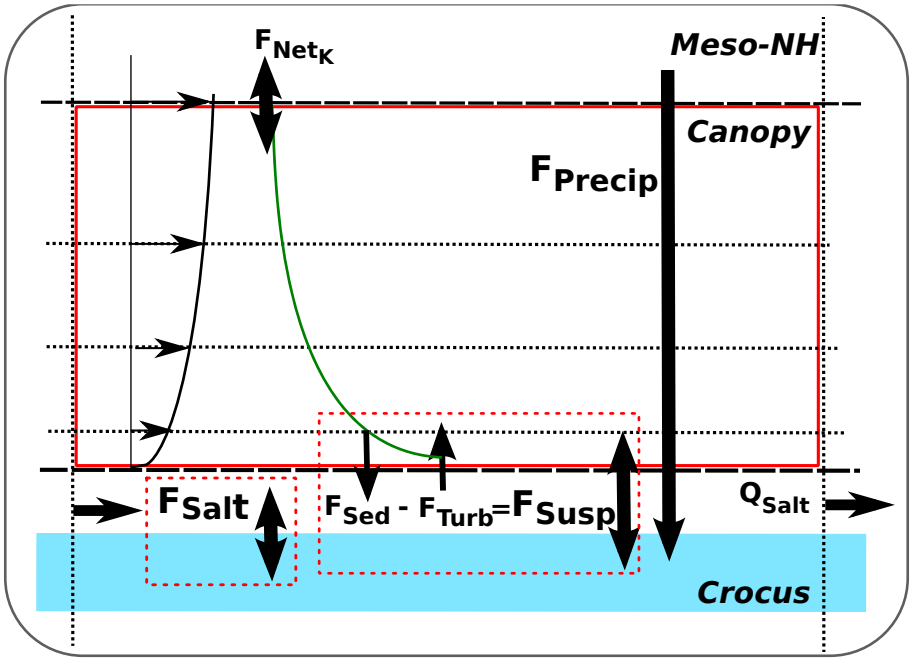

Fig. 2. Mass exchange between the different components of the coupled model Meso-NH/Crocus. The model accounts for snow transport in saltation (F_{Salt}) and turbulent suspension (F_{Susp}) and snowfall (F_{Precip}).

TCD
7, 2191–2245, 2013

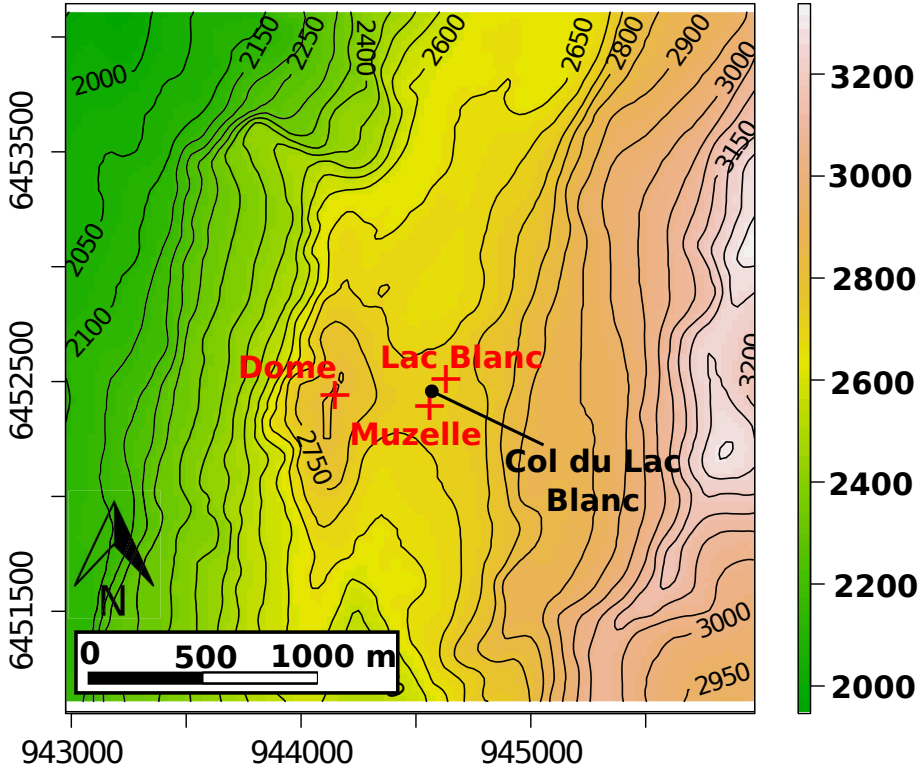

Fig. 3. Map of study site Col du Lac Blanc and the surrounding area. Red crosses indicates automatic weather stations. Meteorological mast and SPC are located at Col du Lac Blanc (black dot). The black isolines correspond to $\Delta z = 50\,\mathrm{m}$.

TCD
7, 2191–2245, 2013

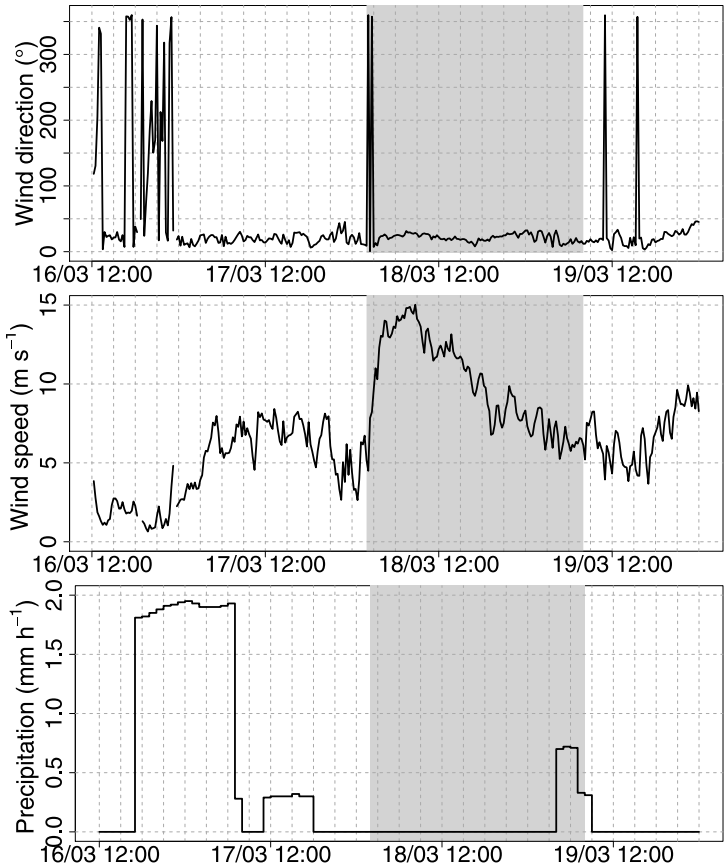

Fig. 4. Times series of observed wind direction (top) and speed (middle) and precipitation (bottom) at Col du Lac Blanc during 3.5 days around our case study (shown in gray). Precipitation are provided by the SAFRAN meteorological analysis system (Durand et al., 1993).

TCD
7, 2191–2245, 2013

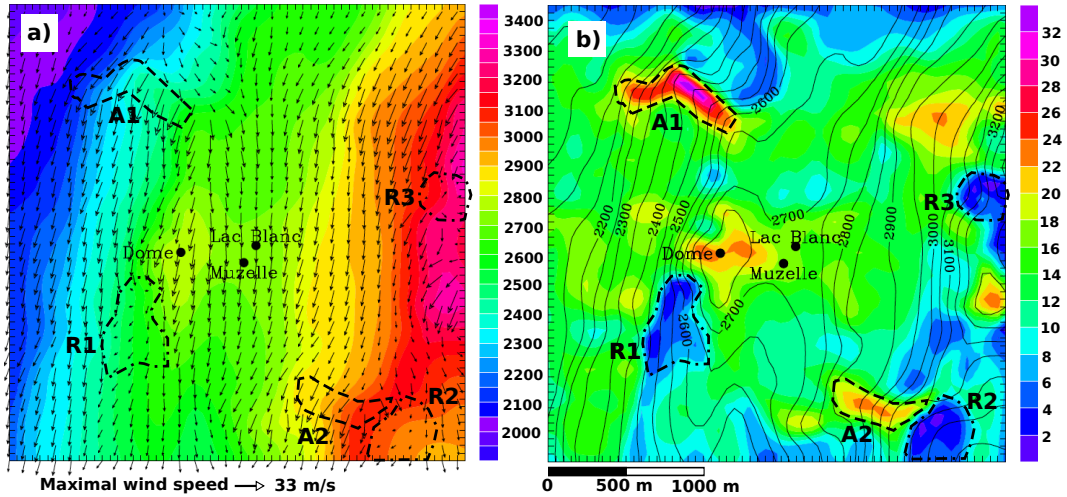

Fig. 5. Wind field at 1st level of Meso-NH (variable height : 1.9–3.1 m) on 18 March 2011 7.00 a.m.: **(a)** wind vectors and **(b)** wind speed. Positions of the 3 AWS around CLB are mentioned on both maps. Properties of wind field in dashed and dashed-dotted areas are discussed in the text.

TCD
7, 2191–2245, 2013

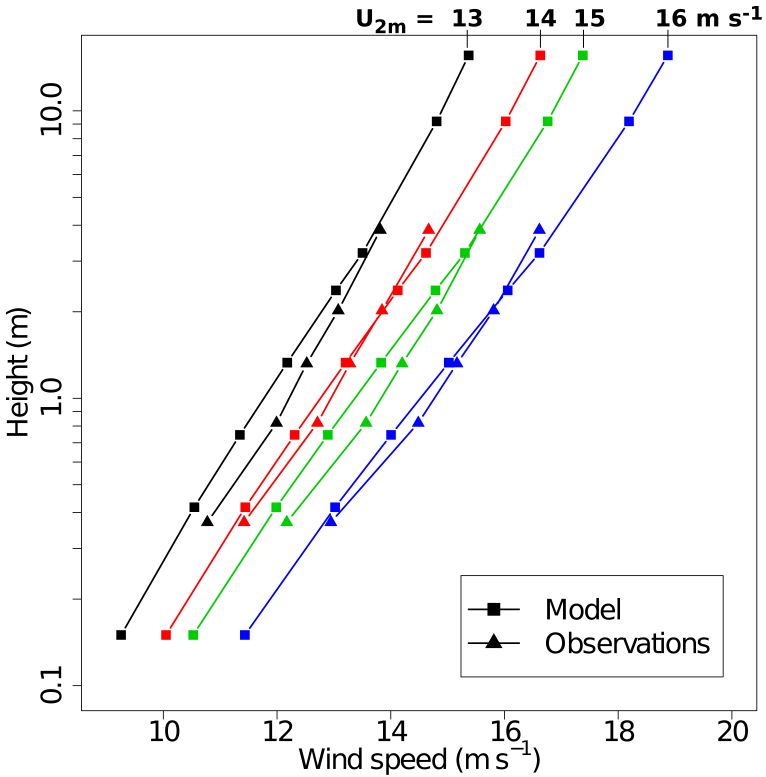

Fig. 6. Comparison between averaged vertical profiles of wind speed simulated by the model and measured on a meteorological mast located at Col du Lac Blanc. Averaged vertical profiles have been computed for 4 categories of 2 m wind speed. Canopy levels refer to the five lowest levels of the model.

TCD
7, 2191–2245, 2013

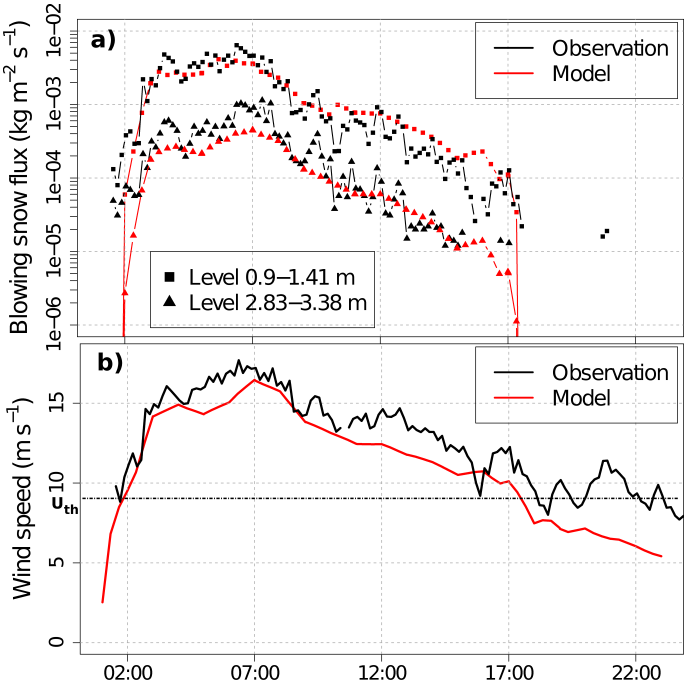

Fig. 7. (a): Blowing snow fluxes simulated by Meso-NH/Crocus and measured by SPC at two levels above the snowpack. Each flux simulated by the model has been interpolated using a power law at the height of the considered SPC. This latter changed during the blowing snow event due to snow erosion and accumulation below SPC. Particles fluxes higher than 100 part cm^{-2} s^{-1} are considered as non-negligible. **(b)**: 2 m wind speed simulated by Meso-NH and measured close to the SPC. The dashed-dotted black line indicates the threshold wind speed, U_{2th}.

TCD
7, 2191–2245, 2013

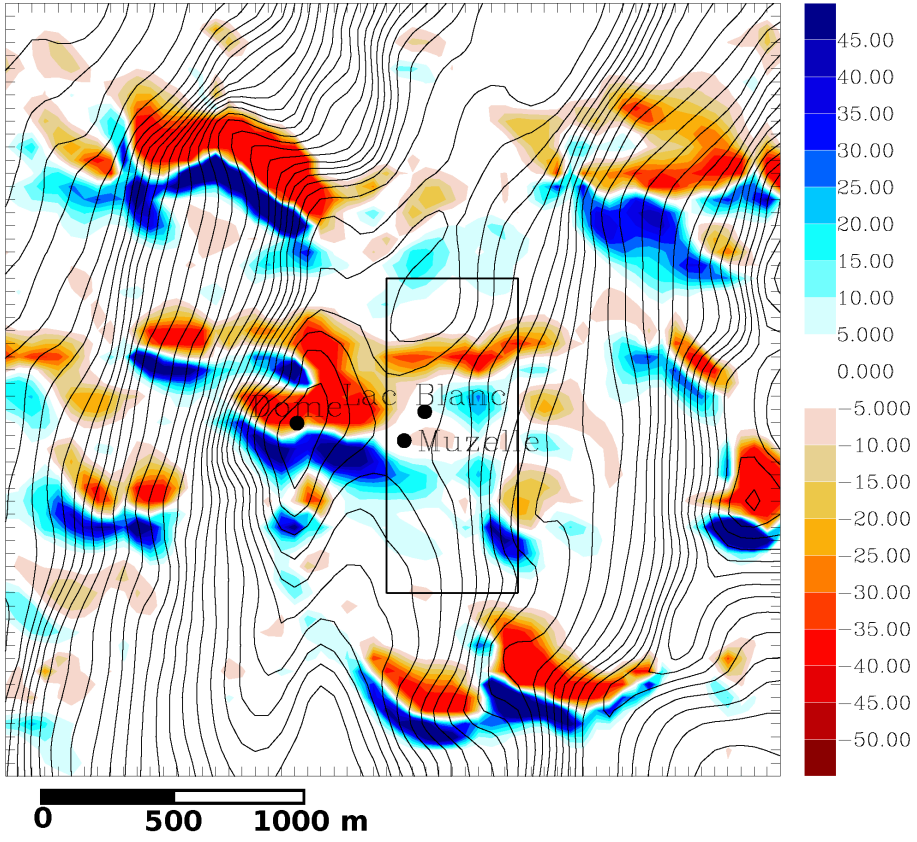

Fig. 8. Map of snow water equivalent (SWE) difference simulated by Meso-NH/Crocus between 11 p.m. and 1 a.m. on 18 March 2011. Black isolines correspond to $\Delta z = 25$ m and black box designates the area where data from terrestrial laser scanner are available.

TCD
7, 2191–2245, 2013

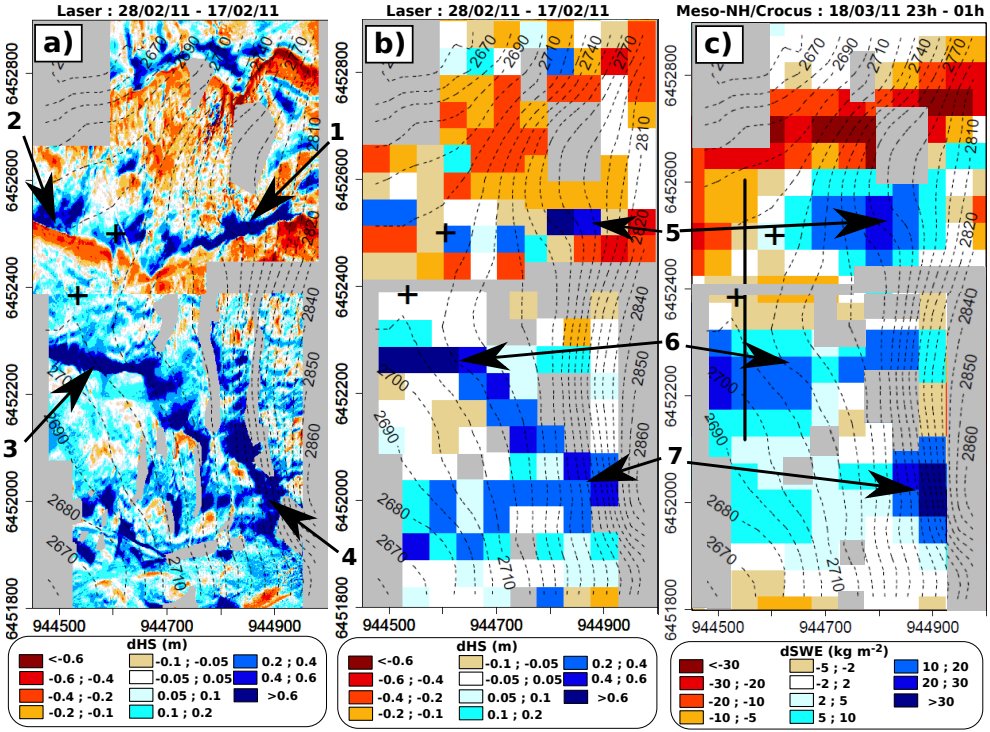

Fig. 9. Maps of snow cover evolution during Northern blowing snow events around Col du Lac Blanc (black box on Fig. 8): **(a)** snow depth difference measured by TLS at an horizontal resolution of 1 m between 28 February 2011 and 17 February 2011, **(b)** same as **(a)** but averaged at an horizontal resolution of 50 m and **(c)** SWE difference simulated by Meso-NH/Crocus between 11 p.m. and 1 a.m. on 18 March 2011. The arrow indicate example of snow deposition patterns discussed in the text. Note the difference of colorbars. The spatial coordinates are in m and the dashed isolines correspond to Δz = 10 m.

TCD
7, 2191–2245, 2013

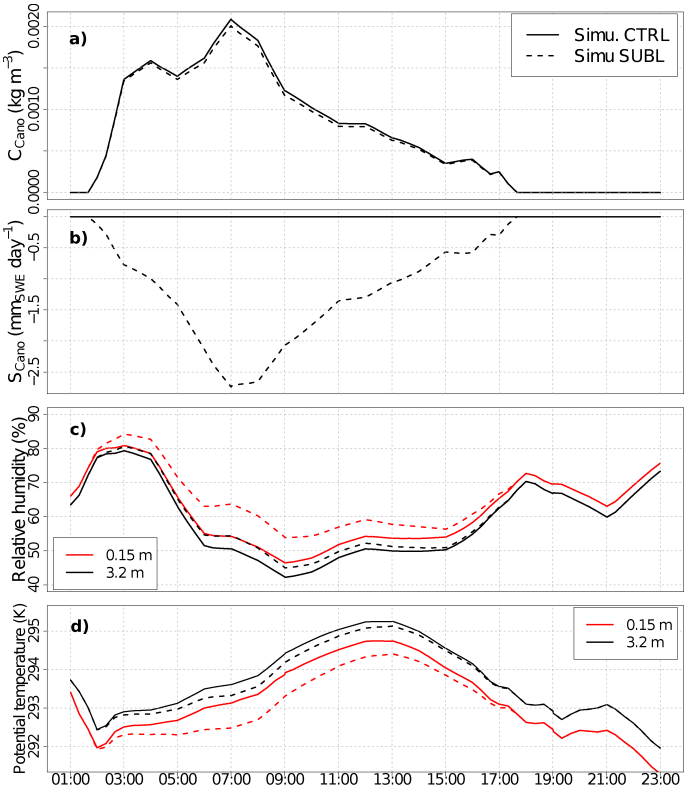

Fig. 10. Times series simulated at Col du Lac Blanc of **(a)** average concentration of blowing snow in Canopy; **(b)** vertically integrated sublimation rate in Canopy; **(c)** relative humidity with respect to ice at two levels and **(d)** potential temperature at two levels. Plain and dashed lines refers respectively to simulation CTRL and SUBL. The total thickness of Canopy is 3.05 m at Col du Lac Blanc.

TCD
7, 2191–2245, 2013

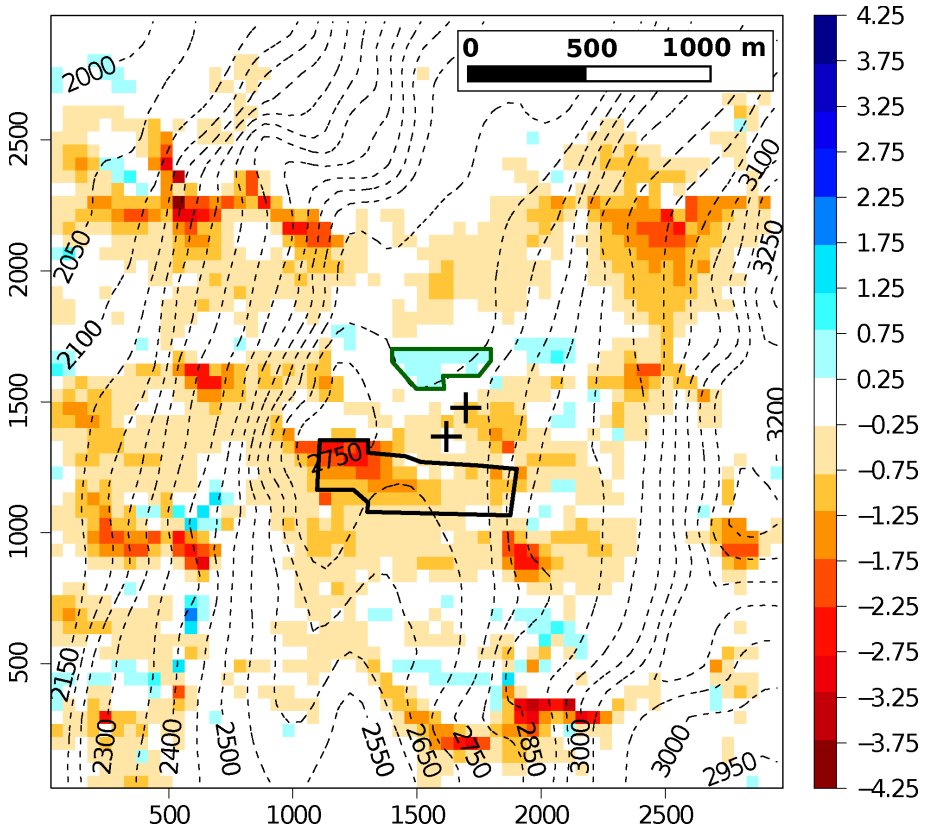

Fig. 11. Difference of SWE (mm_{SWE}) at the end of the blowing snow event between simulations SUBL and CTRL. The black box delineates the area whose mass balance is given in Table 3 while features of the region surrounded by the green box are discussed in the text. The spatial coordinates are in m and the dashed isolines correspond to $\Delta z = 50$ m.

TCD
7, 2191–2245, 2013